COHERENT DEBLURRING TECHNIQUES

A thesis submitted for the degree of

Doctor of Philosophy

by

Ram Mohan Vasu

The University of Aston in Birmingham
Department of Physics

July 1980

This thesis is reverently dedicated to the glory of our Lord Jesus Christ Who alone sustained me throughout my stay in Britain.

Candidate's Name Ram Mohan Vasu

Title of the Thesis Coherent deblurring techniques

Degree Doctor of Philosophy

Year: 1980

Summary

Experimental realization of Fourier plane filters for use in a coherent optical deblurring system for pictures affected by space-invariant blurs is discussed. Linear motion blur and defocusing are the two types of blurs considered. A method of developing phase-inverting filters as diffraction gratings is given. The amplitude filters to go with the phase-inverting filters are developed as density variations on photographic films. The results of deblurring both linear motion blurred objects and out-of-focus pictures are presented and the degree of deblurring achieved is discussed. It is found that increasing the noise term in the amplitude filter results in loss of resolution in the deblurred output. Linear motion blurred object is then processed with an 'amplitude only' filter after subjecting the input object to a further blur of the same nature and amount as the original blur. Deblurring filters are also developed as binary holograms and the deblurred outputs presented and discussed. Loss of resolution in the output due to coarse amplitude quantization levels in a binary hologram filter is reduced by splitting the amplitude part of the filter into two halves and having only one of the halves encoded in the binary hologram filter while the other is produced as a photographic density variation. A simple optical method of enhancing the space-bandwidth product of the binary hologram filters helps to reduce plotting costs while processing large objects.

Index heading : Coherent deblurring, Spatial filtering, Wiener filtering, Binary hologram filter, Double-phase hologram filter.

CONTENTS

LIST OF ILLUSTRATIONS

Acknowledgements

I am very much indebted to Professor G. L. Rogers, my research supervisor, for his encouragement and many stumulating suggestions during the course of this work.

I would like to express my deep sense of gratitude to my colleague, Mr. R. L. Silva, for the many interesting discussions I had with him. The assistance I received from him during the final stages of my experimental work and thesis preparation merit particular mention.

I am grateful to Dr. P. M. Nelson of Atlas Computer Laboratory, Chilton, for introducing me to the use of FR80.

The kindness and understanding shown by Mr. H. Arrowsmith, of the Physics Department workshop, is acknowledged with thanks.

I am thankful to the Association of Commonwealth Universities (London) for the financial assistance I received during my stay in Britain.

I would also like to thank Professor S. E. Hunt in whose department this work was carried out.

Finally, if this thesis is in a presentable form it is due to the patient and skilled typing of Mrs. D. G. Hill.

CHAPTER 1

INTRODUCTION

Section 1.1 General Introduction

Coherent Optical Data Processing systems are found to be capable of achieving certain restricted class of operations such as Fourier transforms, Fresnel Transforms and convolutions. Due to the parallel processing capability of a lens system which incidentally forms the main part of an optical processing device all these operations can be carried out in parallel at the speed of light. Utilizing such capabilities of optical systems three major fields have come to prominence : (i) Optical image deblurring (ii) Coherent side-looking synthetic-aperture radar and (iii) Correlative pattern recognition[1]. We in this thesis are concentrating on the implementation of image deblurring through coherent optical systems.

As the name implies, image deblurring entails generating from a blurred unsharp photograph as fully sharp and enhanced a picture as possible. Looking at a blurred photograph one is tempted to think that most of the information from the original scene is lost forever. But, on the contrary, most of the information is still present in the blurred picture, only in a coded form. Deblurring is essentially a decoding process which aims at a faithful recovery of the object scene from the coded (blurred) picture. At this point it is worth noting one of the limitations of any deblurring procedure: it is impossible to achieve an ideal 100% recovery, as almost all the blurring processes involve irrecoverable loss of some of the information from the object

scene.*

A mathematical function which can be used to represent the impulse response of the optical system under conditions of blur is known as the blur function of the system. In its simplest form it represents a blur that is space-invariant and involving only linear transformations. (A system is said to be space-invariant if its impulse response remains unchanged in shape on varying the position of the input). However, we do encounter in practical situations space-variant and non-linear blurs (a picture taken with a camera under acceleration provides an example of non-linear blur). Powerful digital techniques are available to correct space-variant blurs. Sawchuk[3] describes a method of correcting space-variant blurs by decomposing them to a series of space-invariant blurs. Those class of space-variant blurs that can be reduced to a space invariant blur by a pre-processing transformation can be dealt with by both digital[4] and optical methods [5,6]. We, in this thesis are limiting our attention to space-invariant blurs which involve only linear transformations.

In recent years we have seen a flurry of activity in the field of image processing, with a view to evolve methods for getting high quality output with low costs. The various possibilities that exist can be broadly categorised under two heads : (i) digital[7-10] and (ii) Optical [11-14]. The digital methods are mainly computer assisted

* However, recently it has been pointed out that there is a definite possibility of complete recovery through the use of prolate spheroidal wave functions. (For details see Reference 2)

and are in general done through transformation into the frequency plane. The basic steps involved in such a decoding are (i) digitization (microdensitometer) (ii) transformation into the frequency plane (computer) (iii) spectrum correction(computer) (iv) retransformation (computer) and (v) reconstruction of the output (TV screen). Digital techniques have produced some excellent results and are highly flexible with capabilities of producing many non-linear transformations. When it comes to correcting space variant blurs in particular, because of the broad range of operations possible through computer, digital methods have proved to be superior to any optical methods that can be envisaged. (Apart from the frequency plane correction method described above some iterative algorithms are also in existence for use in computer aided picture enhancement [15-16]. Rapidly converging algorithms have helped reduce the computation time involved and have at the same time produced results of comparable quality.) The 'transform-operate-inverse transforms' process has become more attractive after the invention of the Fast Fourier Transform algorithm[17] which has reduced the computation time by a factor of $N^2/N\log_2 N$. The high level of noise suppression achieved is another advantage of digital methods that is worth mentioning.

In spite of all that is said above, digital methods do have some serious disadvantages. First of all, they are very expensive and need incredibly large storage facilities and fairly high computation times. This is particularly obvious when processing objects with large space-bandwidth product. Secondly, sequential mode of operation of computer makes digital methods relatively inefficient. (Highly advanced computers are available today which possess a limited parallel processing

capability). Also there is a certain amount of unavoidable error due to digitization of the input picture.

An alternative approach to this problem of picture enhancement would be, as noted earlier, by analogue (optical, both coherent and non-coherent) means. The coherent optical implementation of a 'transform-operate-retransform' picture processor is quite easy and inexpensive so long as we are limiting our blur function to the space-invariant type. For space-variant blurs coherent optical solutions have been envisaged[5 6], but the methods are not easy and the results are not comparable with those from digital techniques for the same blurs. For space-invariant blurs the blurred picture is represented as a convolution integral between the original object and the blur. Such a blurred picture on Fourier transformation produces a spectrum which is a product of the original object spectrum and the transfer function of the blur. With coherent illumination Fourier transformation is easily carried out by a lens. The effect of the blur transfer function can easily be annulled, to a degree, by allowing the Fourier spectrum (of the blurred picture) to pass through an appropriate filter. This filter is designed after taking into account the type and amount of the blur the original picture has undergone, illumination wavelength and the focal length of the lenses used in the processing system. The corrected spectrum is recombined (again using a lens) to form the 'deblurred' image.

As mentioned before, this method is very easy and many people have successfully generated filters for correcting various kinds of blurs. (We defer a closer look into the various methods that are available at present for filter fabrication to a later paragraph of this chapter).

As opposed to digital methods, optical systems have parallel processing capability at the speed of light and this is by far the greatest attraction of an optical processor. But we must point out that the quality of outputs obtained from a coherent optical processor is not as high as that from a digital image processor. However, coherent deblurring can be a worthwhile first stage operation (basically to reduce the cost involved) before the final enhancement is done through a computer. The main drawback of a coherent system is its inherent noise. The noise is mainly due to the following two reasons : (i) a coherent system is non-redundant[18] and hence noise encountered in any part of the system (e.g. a film of dust in any one of the lenses) becomes inseparable from the output image (ii) photographic emulsions are always used to both input information into and record the output from a coherent system. Graininess in the emulsions causes scattering and is another source of noise. Processing of signals in the presence of noise has necessitated certain assumptions regarding the nature of noise and also led to setting up of some criteria for best processing. For example, photographic grain noise on an input recording is considered as a signal dependent, multiplicative noise [19]. The Wiener filter [20] which is arrived at by requiring that the mean squared error between the recorded image and the ideal object is minimum can be cited as an example utilizing a convenient criterion.

Extensive work on the cause and the nature of noise in coherent optical systems has already been done and it is not our intention in this thesis to go into this problem in any detail. However, we would like to note that Wiener filtering has reduced a great deal the

problem of system noise in coherent deblurring.

The main contribution of this work is developing various ways of implementing a Wiener filter processor.

(There is another way of greatly reducing the problem of noise in optical processors. That is by replacing coherent illumination with a spatially noncoherent illumination. As a noncoherent processor is highly redundant, local blemishes and other sources contributing to noise only lowers the overall contrast of the output. Since a noncoherent system deals with only intensity values the point spread function of the system is limited to be wholly positive. This curtails the use of non-coherent systems in cases involving complex impulse responses. However, in recent years there has been a good number of publications that look into the possibility of processing complex blurs by noncoherent processors[21-25] .)

As already noted, design and fabrication of a suitable filter for modifying the object spectrum is the most important step in a coherent deblurring experiment. Abbe [26] by his explanation of image formation through diffraction has indicated the possibility of spatial filtering for image modification as early as 1873. Subsequently, in 1935 Zernicke[27] made use of this idea in his phase-contrast microscope for imaging phase-objects. A deblurring spatial filter in the general case, should be able to modify both the amplitude and phase of the object spectrum and, hence, should have in general a complex transmittance function. Maréchal and Croce [28] generated a purely attenuating filter which corrected only the amplitude part of the spectrum. With that he was

able to improve the contrast of a photographic image.

Tsujiuchi[29] by sandwiching an attentuating part and a phase shifting part fabricated a complex deblurring filter for correcting out-of-focus pictures. The phase-shifting part was made by vacuum deposition of aluminium in sufficient quantities to retard light used in the experiments by half the wavelength. The phase shifts were effected in alternate annular regions in a good quality glass plate. The attenuating part was made using a photomechanical technique by photographing an illuminated rotating mask which has a completely transmitting region on an opaque background. The profile of the transmitting region is so designed that it generates on rotation a desired intensity pattern. This pattern is converted to an amplitude transmittance variation on a photographic film by a suitable photographic process. Holladay and Gallatin[30] describe a method of generating phase filters with 0° and 180° regions, using polarized light and photographic printing. Though this filter is originally designed for matched filtering, it can well form the phase part of a deblurring sandwich filter. Mountain [31] has recently shown that a photoresist relief image can be used to retard phase in a controlled fashion. He has, since then, calibrated the phase shifts with respect to a number of experimental parameters involved in generating the photoresist image and has generated photoresist phase filters for out-of-focus picture correction.

With the advent of holography many holographic deblurring filters were proposed and implemented [32-36]. The development of a holographic spatial filter for matched filtering was first reported by Vander Lugt[37] Subsequently, the method was developed to a considerable extent by such

workers as Stroke[38], Tsujiuchi[39] and Krusos[40]. Holographic technique is applicable only if the point spread function of the blur is readily available. If this is the case, a holographic filter for application in image deblurring is easily constructed, starting from the image of a blurring point spread function.

However, since the blur transfer functions have a very large amplitude range, photographic processes for recording the holograms were found to be inadequate. This is due to insufficient linear range of the photographic emulsion. Stroke and Halioua [41] found a method of getting round this problem, by recording the amplitude part of the deblurring filter separately on a combination of two photographic emulsions which, together, gave a linear range sufficient to accommodate the amplitude variation. Goodman [42] came up with yet another solution by modulating the input and the blur point spread function with a transmission grating. By doing so, the corresponding Fourier spectrum was divided into a series of Fourier coefficients, each coefficient having a range small enough for being recorded in the linear range of the photographic film used. By developing an exposure device controlled by a nonlinear amplifier Minemoto [43] was able to correct the effect of film nonlinearity. Consequently he was able to utilize the entire dynamic range of the film, not just that portion where the characteristic curve is linear. Ragnarsson [44] reported the fabrication of a Wiener deblurring filter for defocusing as a single hologram. The hologram, which was formed using a weak reference beam, was bleached and had produced a deblurring filter with a significantly large linear response. This filter was also found to be automatically optimum with respect to granularity noise in the input image.

With the introduction of large computers and efficient high resolution plotters,it was possible to generate digital holograms through computer. Particularly interesting are binary holograms with only two levels of amplitude transmittance, either zero or one. These binary holograms are easy to fabricate and are a quantized (and hence approximate) representation of a complex wavefront. Lohmann and Paris[45] utilized binary holograms, for fabricating filters for many optical data processing applications. One of the main advantages of computer generated holograms is the fact that any mathematically defined filter function, not necessarily having a realizable point spread function can be generated using a computer. Friesem and Peri[46] have generated Wiener filters, for correcting out-of-focus pictures,as Lohmann holograms. Apart from the fact that a Lohmann hologram spatial filter is only an approximate digital representation of a continuous function, it has two major practical limitations. First, when used to process large objects, the filters should have a space-bandwidth product at least as large as that of the object. Consequently, production of computer-generated filters involves very large computing and plotting time and hence can be expensive.

A suggestion for bringing down the computing time was put forward by Lowenthal and Chavel[47] and was made use of by Friesem and Peri in their work described in reference.[46] Lowenthal and Chavel's method involves producing a high space-bandwidth product 'natural hologram' filter by combining a reference beam at an appropriate angle with the image produced by only the first order spectrum from the low space-bandwidth product computer generated spatial filter.

The second serious limitation of a Lohmann hologram is its inability to code low amplitude values in the filter. This is due to the limit imposed by the plotter-pen resolution on the minimum amplitude value that can be coded. We address this problem in Chapter 6 which gives a detailed analysis of computer generated binary holograms with special emphasis on application to spatial filtering.

As opposed to the above mentioned method of image enhancement by what is essentially 'Fourier transform division' filtering, there are two other methods worth mentioning not involving Fourier transformation. The first is by performing a further convolution on the blurred picture; the new convolution kernal is so designed that it convolves with the blur point spread function to give a δ-function. Tsujiuchi and Honda[48] describe an interesting analogue electrical deblurring technique for motion blurred objects. They use a scanning technique and the scanning impulse response is derived by Fourier transforming the inverse of the blur transfer function. For motion blur, the scanning deconvolution is easily achieved, since the scanning impulse response is a binary function and is readily fabricated. This idea is utilized by Fleuret, Maitre and Cheval[49] for making a Fourier-transform division filter for optical deblurring. The starting point is the deblurring impulse response, which has a simpler form, and the Fourier plane filter is produced as a Fourier transform hologram.

The second non-Fourier plane deblurring experiment is described in a paper by Peri and Friesem[50] recently. Enhancement is achieved by a space (object) plane filter. The filter is fabricated as a volume hologram which has a selective angular diffraction efficiency.

Since diffraction angle in the object plane has the same meaning as spatial frequency in the Fourier plane, a volume hologram with properly controlled angular diffraction efficiency variation can effect the same spectral modification as a Fourier plane inverse filter. As this method does not require intermediate Fourier plane processing, with short focal length imaging lens, a compact optical system is produced. As grating filters located in the object plane do not produce dispersed images, white light processing capability is another advantage of the method.

The present work is mainly practical implementation of optical Fourier plane deblurring filters for blurs due to linear motion and defocusing. The second section of this chapter gives a brief mathematical introduction to optical deblurring. In Chapter 2 we describe a method of generating 'phase-filter'as a diffracting grid. The 'amplitude' part of the deblurring filter for linear motion blur is developed in Chapter 3. The 'amplitude' filter for correcting out-of-focus picture is developed in Chapter 4. In Chapter 5 we have deblurred a motion-blurred picture by a positive only filter after having subjected the blurred picture to a further blur of the same nature and amount. Chapter 6 gives a detailed analysis of binary holograms. We look at their application to image deblurring and consider their limitations. We summarise the main developments of this thesis and give our concluding remarks in Chapter 7.

Section 1.2.

Mathematical Preliminaries.

The theoretical background of optical spatial filtering is well know

However, for the sake of completeness we give a brief outline of the mathematics involved.

Formation of a blurred photograph (for that matter any photograph, blurred or sharp) can be described, in general, by the superposition integral

$$g(x,y) = \int_{-\infty}^{\infty}\int f(x',y')\, h(x,y;x',y')\, dx'dy' \qquad \ldots\ldots\ldots\ldots (1.1)$$

where g(x,y) and f(x,y) are the image and object intensity distributions respectively and h(x,y) is the impulse response of the optical system.

For certain types of blurs, which include linear motion of the camera and defocusing under the assumption that the picture occupies only a limited region of the field, Eqn 1.1 can be simplified to a convolution integral :

$$g(x,y) = \int_{-\infty}^{\infty}\int f(x',y')\, h\,(x-x',y-y')\, dx'dy' \qquad \ldots\ldots\ldots\ldots (1.2)$$

In the Fourier plane Eqn 1.2 can be written as

$$G(v_x,v_y) = F(v_x,v_y)\;\; H\;(v_x,v_y) \qquad \ldots\ldots\ldots\ldots (1.3)$$

where G,F and H are the Fourier transforms of g, f and h respectively.

By passing Eqn 1.3 through a filter with transmittance proportional to $\frac{1}{H(v_x,v_y)}$ we can recover $F(v_x,v_y)$ completely provided H never goes to zero within the region where $F(v_x,v_y) \neq 0$.

But unfortunately this is not the case in most of the practical situations and the image recovered by spatial filtering is seldom perfect. Moreover, since $H(v_x,v_y)$ in almost all the cases is found to decrease rapidly with frequency , $\frac{1}{H(v_x,v_y)}$ has the undesirable effect of enhancing high frequency noise in the image. The filter should ideally be of infinite lateral extent, which obviously cannot be achieved. The higher the number of lobes, the bigger the contrast of the filter which means higher densities in the central region of the filter which pushes up the deblurring exposure time. $\frac{1}{H(v_x,v_y)}$ has infinities at cross-over points (i.e. where $H(v_x,v_y)=0$) and in practice we can only have approximations to it.

These drawbacks are overcome to an extent by replacing $\frac{1}{H(v_x,v_y)}$ by what is known as a Wiener filter [20] which has been arrived at using a Least Mean Square Error criterion between the ideal object and the recovered image. In the Fourier plane, the Wiener filter has the form $H^*/(H^2 + \varepsilon)$ where H^* is the complex conjugate of H and ε is the ratio between noise and signal(object)power spectral densities. The Wiener filter has no infinities in it because of ε and hence there is no need of approximations while fabricating. Also because of ε it is laterally self limiting. Compared with the inverse filter, Wiener filter has a limited amplitude range.

The filter function, either $\frac{1}{H}$ or $H^*/(H^2 + \varepsilon)$ which in general has a complex transmittance function, can be expressed as $H_{amp}e^{i\phi}$ where H_{amp} is a purely amplitude modulating part (hereinafter called amplitude filter) and $e^{i\phi}$ a purely phase modulating part (hereinafter

called phase filter). In Chapters 2, 3 and 4 of this work we present how we developed the final filter function as a sandwich between the amplitude and phase filters which are made separately. In Chapter 6 we developed the filter as binary holograms representing both the amplitude and phase parts simultaneously in the same hologram filter.

C H A P T E R 2

THE PHASE-INVERTING GRID : ITS CONSTRUCTION

Section 2.1. Introduction

A blur transfer function can be in general complex. However, in certain cases of blurs, with circular or line symmetric point spread functions (e.g. linear motion blur and defocusing) the blur transfer function is real, but not wholly positive. Hence the correcting filter function should be able to fulfil two requirements : (i) attentuate the object spectrum in such a way that the modulus of the blurred object spectrum resembles as closely as possible to the modulus of the unblurred object spectrum; (ii) effect phase inversion in those frequency regions where the blur transfer function has negative values. It is common practice to develop the correcting filter as a sandwich of two parts, one a purely attenuating part (called the 'amplitude filter') and the other a phase shifting part (called the 'phase filter'). In some of the deblurring experiments described in this work, we follow a similar approach and fabricate the amplitude and phase filters separately. In this chapter we describe how we develop phase filters as diffraction gratings, for linear motion blur and defocusing.

The principle of a diffraction grating phase filter is that it introduces phase changes by 'detour phase variation'in the diffraction image as first pointed out by Lord Rayleigh. This detour phase coding is utilized by Lohmann[56] for representing phase in a computer generated hologram. As our blur transfer functions here are real (having only positive and negative values) our correcting filters need have only two

phase values, 0 and 180°. In a grating phase filter, as we move from a positive region (0°phase) to a negative region (180° phase) the lines in the grating shift in position by half the period of the grating. The useful image (here,the corrected picture) is observed either in the +1 or -1 order spectrum of the grating.

Stroke et al [57] generated a phase-shifting grating by using a computer plotter to draw a master grating with appropriate phase shifts. The performance of such a grating depends, a great deal, on the positioning accuracy of the plotter pen and also on the uniformity of ink-flow in the pen. Moreover, production of a large space-bandwidth product filter using the plotter is time consuming and hence, expensive. However, Chavel and Lowenthal[47] have suggested a method of producing a large space-bandwidth product filter from a computer generated low frequency filter by optical heterodyning.

We here generate our grating optically on a high contrast 'switching' film using a lenticular grid and a rectangular light source.

SECTION 2.2. A square-wave grating with lenticular grid and high contrast film.

A lenticular grid is a series of good quality perspex cylindrical lenses placed side by side on a perspex base. The separation between the cylindrical lenses is typically 0.3 - 0.5 mm and the overall thickness of the grid (including the base)is about 3 mm. A diffuse source of light set in front of the lenticular grid produces, by the cylindrical lens effect, a series of light stripes in the image plane of the

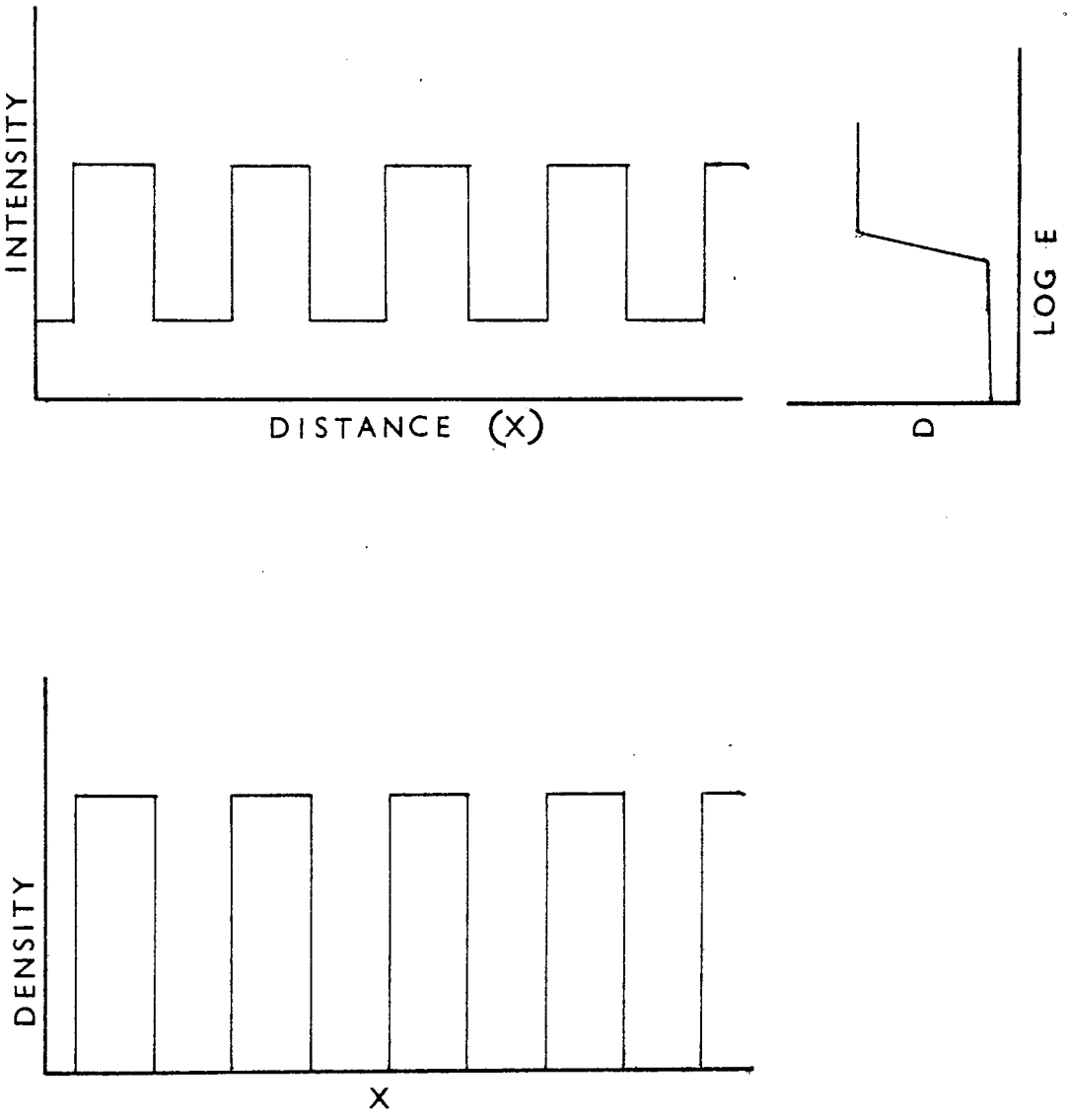

Fig.2.1. The switching nature of the recording film is used to generate the black and white grid. The background intensity due to scattering is not recorded.

cylindrical lens[18]. Across each stripe there is an intensity variation proportional to the geometrical shape of the diffuse light source used. Using the same principle Jacobs[58] produced a triangular repeated variation of intensity, by having a triangular diffuse source in front of the lenticular grid. By imaging the repeated intensity variation through a continuous tone picture, Jacobs generated a pulse-width modulated carrier wave picture of the same continuous tone object. The pulse width modulated picture was produced on a 'switching' film. The point of switching due to the triangular intensity variation (and hence the width of the opaque line generated) depends on the optical density variation in the original continuous tone photograph.

We have used a method similar to Jacob's pulse-width modulated photography to generate a square wave grating. In our case, we do not want a pulse-width variation across the grating; instead the line-width should be as constant as possible. We have achieved this by replacing the triangular source in Jacob's experiment by a square-topped source. The square-topped source is imaged onto a high contrast film through a lenticular grid of the same frequency as the grating we want to generate. The width of the square-topped source is so adjusted that the rectangular stripes of light generated by the lenticular grid occupy exactly half the lenticular period.

When such a light distribution is recorded on a high contrast switching film, a grating with nearly 1:1 black to white ratio is produced. The point of switching is controlled in such a way that the scattered light forming a bias to the rectangular intensity stripes is not recorded, while the rectangular stripes themselves are fully recorded (see Fig.2.1).

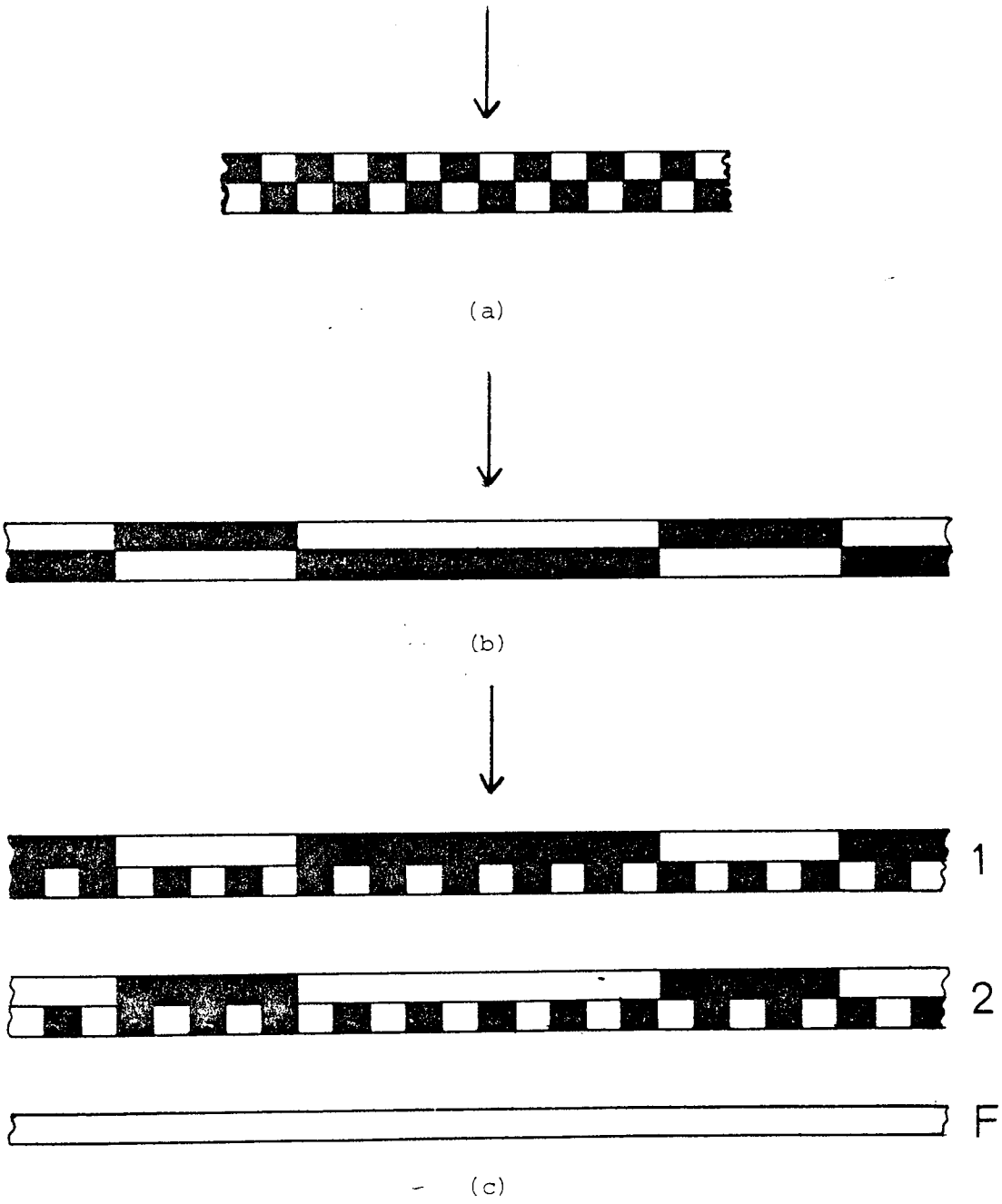

Fig. 2.2 Preparation of (a) the complementary grids, (b) complementary masks and (c) the composite grid: (1: first exposure, 2: second exposure and F:the lithographic film)

We have used this grating, as described in the next section, to generate phase-shifting grids for linear motion blur and defocusing

Section 2.3. Phase-shifting grating from lenticular grid.

The square-wave grating generated from the lenticular grid is printed onto a lithographic film (Fig.2.2a). Both the grating and the lithographic film are punched for a standard registration bar and while printing the film and the grating are registered carefully in the same registration bar. The grating, lithographic film and the registration bar are held in a vacuum printing frame. The lithographic film, after processing, gives a square wave grating which is a complement of the one produced from the lenticular grid. Thus we are able to produce two gratings of nearly 1:1 black-to-white ratio with an 180° phase shift between them.

Two control masks are made on the lithographic film, one the complement of the other, which pass between them the positive and negative regions of the blur transfer function. The second control mask is made from the first by printing using the punch and registration bar to ensure proper registration (see Fig.2.2b). We have made two pairs of control masks, one for the sinc function(which is the blur transfer function for linear motion blur) and the other for $\frac{J_1(r)}{r}$ (the blur transfer function for defocusing, where J_1 is the Bessel function of the first order, first kind.

The phase-shifted gratings are then printed onto a lithographic film, the first grating through one of the control mask and the other through the complementary mask (See Fig.2.2c). Both the printings are done in

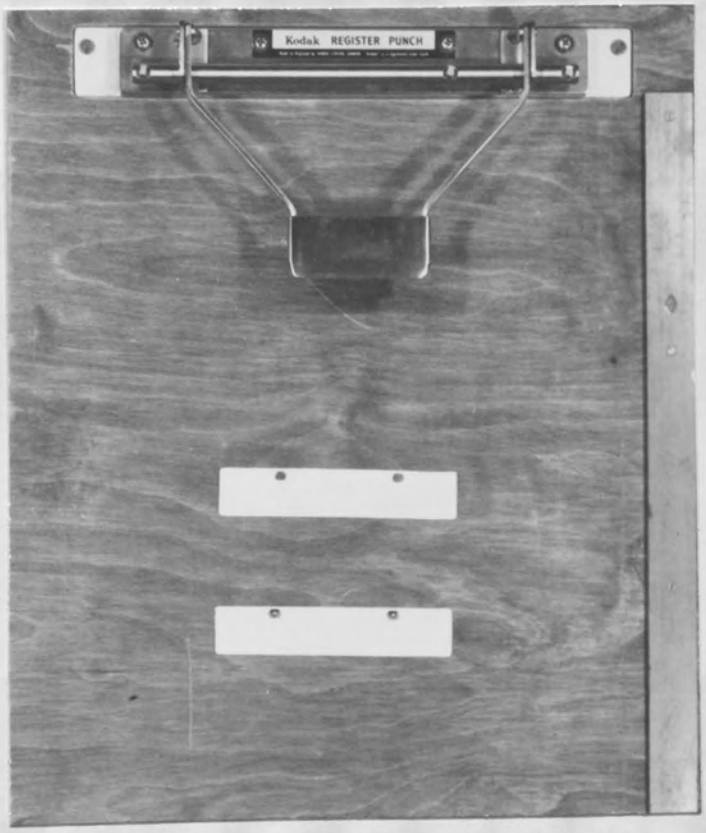

Fig.2.3 Photograph showing the 'Kodak' register punch and pins.

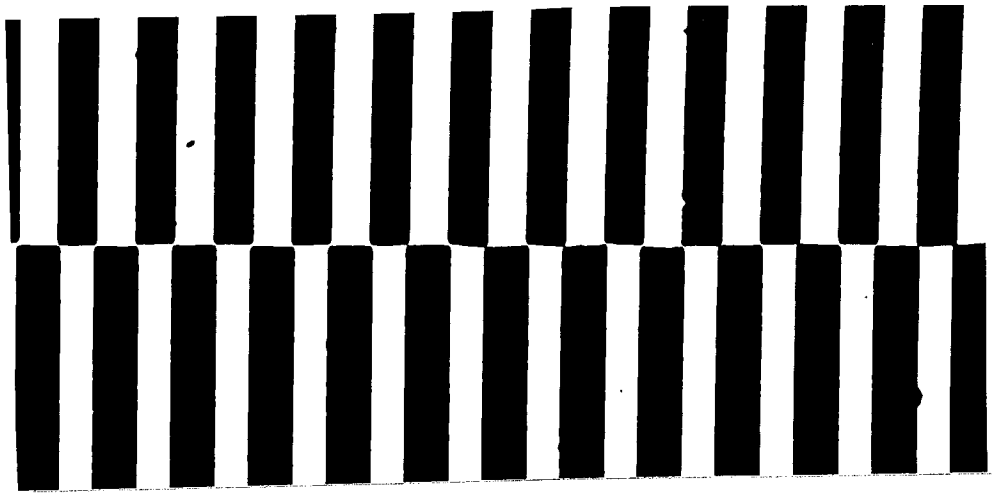

(a)

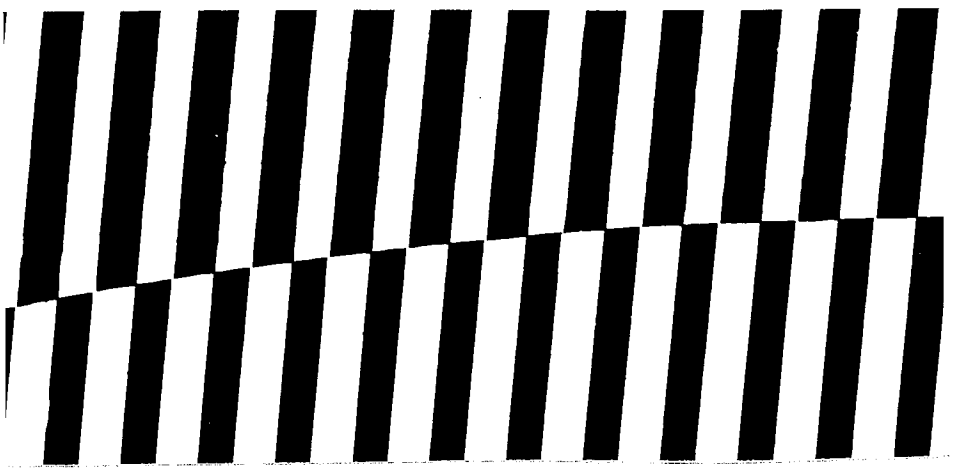

(b)

Fig.2.4 Highly magnified photographs showing a part of the junction between the positive and negative regions of the filter. (a) linear motion blur; (b) defocusing.

a vacuum printing frame with the film, grating and the mask registered well on the registration bar. The composite print so obtained forms the master grating which when reduced onto a high resolution plate gives the final phase filter.

Section 2.4. Experimental.

The exposure and development of the lithographic film for correct switching are found by trial and error and they are maintained the same in all the steps involved. The lithographic film used is Kodalith ortho type 3 (2556). It is developed in Kodalith super developer type A and type B, mixed in the same proportion (diluted 1:3) for 2½ min at 20°C. Great care should be taken against misalignment while taking the composite print. The final grating is carefully checked under a microscope for registration.

The punch and registration bar are made by Kodak, a photograph of which is shown in Fig.2.3. For details, see Kodak Art Reference leaflet 'GA-Ref 7'.

In the case of linear motion blur the master grid we made is about 200 mm wide and has about 500 lines in it. The master grid for defocusing is about 75 mm in radius with about 375 lines. The black-to-white ratio we could get was not exactly 1:1. However, since the black-to-white ratios in the positive and negative regions of the filter are complementary, the diffraction efficiency of the regions is the same. An enlarged version of the part of the filters (for both linear motion and defocusing) containing a junction between the positive and negative regions is shown in Fig. 2.4.

Slight non-uniformities present in the master grids were accentuated by the high contrast nature of the Agfa 10E75 or 10E56 plate onto which they were reduced. We overcome this difficulty by combining the mastergrid with its own unsharp copy made with an average contrast of slightly less than one. (The unsharp copy was made in Ilford Technical Orthochromatic film, using Ilford ID11 developer). This corrected the low frequency drift in the master grid and the reductions from it were found satisfactorily uniform .

The final grating for linear motion blur was about 7.7 mm across with a spatial frequency of about 65 lines mm^{-1}. The corresponding values for the defocusing filter were 8.00 mm and 63 lines mm^{-1}.

C H A P T E R 3

THE AMPLITUDE FILTER FOR LINEAR MOTION BLUR

Section 3.1. Introduction

In Chapter 2 we discussed the construction of a 'phase filter' which forms one part of the sandwich deblurring filter. As mentioned there, the second half of the sandwich filter is a purely attenuating part, which we call the 'amplitude filter'. The amplitude filter is designed to cancel the effect of the modulus transfer function of the blur on the object spectrum. In this chapter we describe a method of fabricating amplitude filters for linear motion blur, as a density variation on photographic films. The method described here is applicable only when the blur transfer function is one dimensional. The amplitude filter for 2-d and circular symmetric blurs is developed in Chapter 4.

Stroke et al[12], in their work on constructing sandwich filters using holography, describe, among other things, a method of generating the amplitude part of a simple 'inverse filter'. There, it is assumed that the impulse response of the blur is known and is easily realizable optically. (An example is the blur due to defocusing where a transmitting circle on an opaque background is the impulse response of the blur). From the blur impulse response, using coherent optics, the blur transfer function is easily realized as an amplitude distribution in the focal plane of a lens system. By recording the resulting intensity distribution on a photographic plate processed to a suitable contrast index, Stroke et al[12] generated a filter with amplitude transmittance variation proportional to the inverse of the modulus transfer function of the blur.

Obviously this method is limited, in its application, to only generating simple inverse filters. For, in the case of a least-mean-square filter (i.e.Wiener filter) the impulse response is not quite a straight-forward function and is not easily realizable. However, Ragnarsson[44] describes an ingenious Fourier transform method of generating a Wiener filter, as a single hologram, using a non-linear recording process. Way back in 1961 Tsujiuchi [29] had described a photomechanical method of generating the inverse filter for correcting out-of-focus pictures. Subsequently, Stroke et al[57] adapted the same technique for generating Wiener amplitude filters for circular symmetric blurs. The photomechanical technique is quite useful in that it allows, unlike Ragnarsson's method[44], generation of Wiener filters without restriction on the value of the noise parameter ε. This means, a parameter in the hands of the experimenter, that can be set for best deblurred output.

Tsujiuchi's method[29] is suitable when the blur function is circular symmetric and hence cannot be used for linear motion blur. Here we describe a method, which has the flexibility of Tsujiuchi's method, of generating amplitude filters for linear motion blur.

For linear motion blur the impulse response is given by a rectangular function defined as

$$\text{rect}\ (x/a) = 1 \text{ for } |x| < a/2 \qquad \ldots\ldots\ldots\ldots\ldots\ldots (3.1)$$

$$= 0 \text{ otherwise}$$

So the blur transfer function is proportional to $\frac{\text{Sin}x}{x}$. A correcting inverse filter has the form $\frac{x}{\text{Sin}x}$ and the Wiener filter,

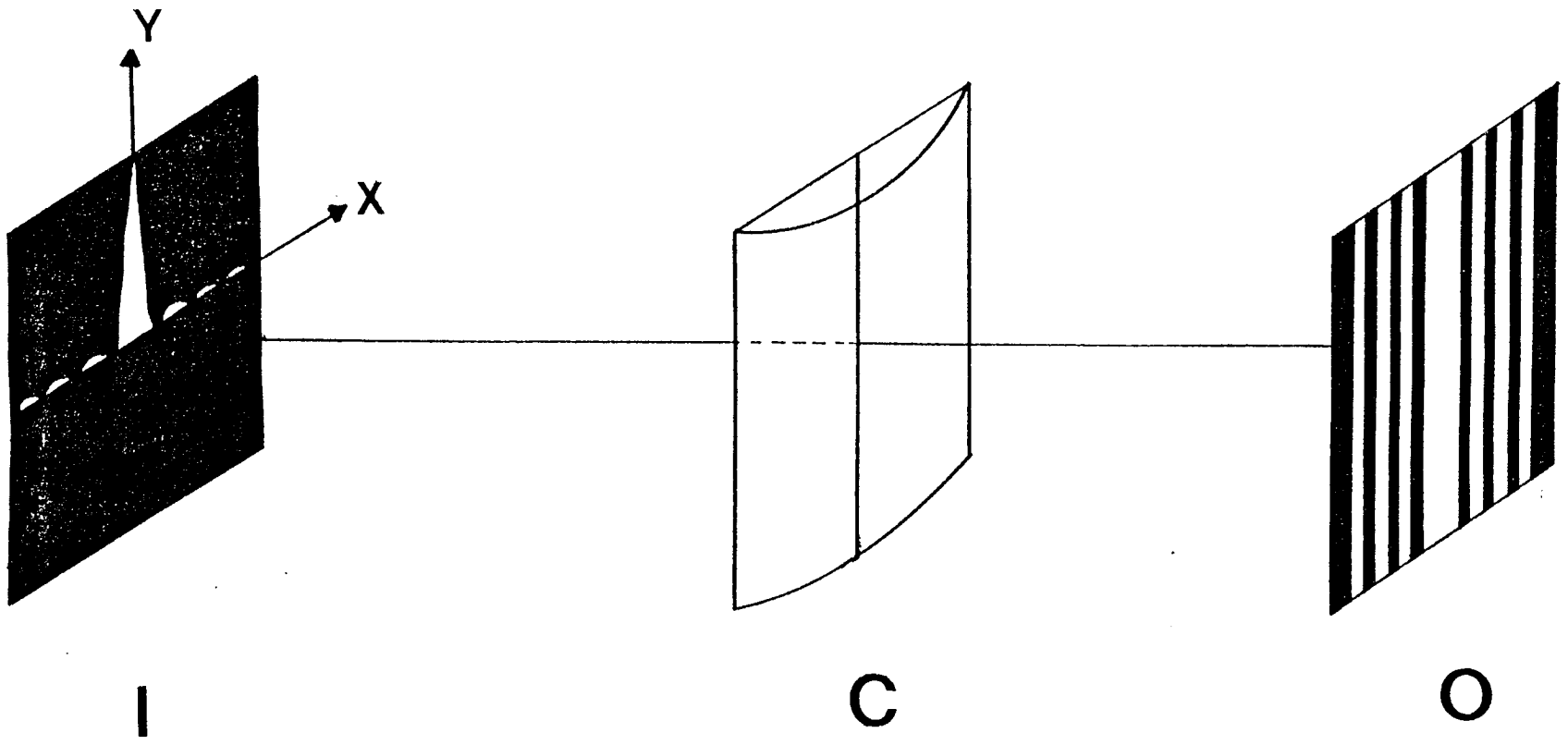

Fig.3.1. The set-up for obtaining the amplitude filter for linear motion blur; a binary transmittance function shown in plane I as an Y-coordinate variation is converted by the cylindrical lens C into a corresponding intensity variation at plane O.

$$\frac{\text{Sinx}}{x} \Big/ \left[\left(\frac{\text{Sinx}}{x}\right)^2 + \varepsilon\right]$$

Section 3.2 Cylindrical lens: Conversion of a mathematical function, represented as a transmitting area variation, into an intensity variation

Rogers[59] in a paper on artificial holograms gives a method of producing continuous tone holograms of 1-d objects using a cylindrical lens. In particular he describes an arrangement for making a hologram for an object consisting of two wires. There, Rogers uses a cylindrical lens imaging system to convert a transmitting area variation in an opaque background (representing the Fresnel transform of the object) to a corresponding intensity variation. A continuous tone hologram is formed by recording this intensity variation.

We use a similar cylindrical lens imaging system to generate an intensity variation proportional to the transmittance of the amplitude filter we want to construct. The principle of the method is described as follows : With reference to Fig.3.1 a transilluminated object O, which has a fully transmitting area between y = f(x) and x-axis in an opaque background is imaged through a cylindrical lens C. Each of the points in any line parallel to y-axis, say OY, is imaged by the cylindrical lens as a line (here OY1) in the output plane O,in the same position. So, the intensity along OY1 is proportional to the height of the opening OY in the object. As a result, the intensity variation in the output plane is proportional to the function represented by f(x) in the input plane. Here we assume that the cylindrical lens has a sharp line spread function which can be

approximated to a δ function. If this assumption cannot be made the design of a black-and-white object is not straightforward and should take into account the spread due to the finite line spread function of the lens.

Assuming that the linespread function of the cylindrical lens is unsharp but stationary, the intensity variation in the output plane I(x),is related to the intensity function in the input plane, O(x) through

$$I(x) = \int_{-\infty}^{+\infty} O(x')L\,(x-x')\,dx' \quad \ldots\ldots\ldots\ldots\ldots\ldots\ldots\ldots\ldots\ldots (3.2)$$

where L is the line spread function of the cylindrical lens.

The nature of the function L can be determined experimentally, to a reasonable accuracy, by imaging a point source through the cylindrical lens. Once the line spread function and the output intensity to be generated are known, Eqn 3.2 can be solved for O(x), the input plot.

A Fourier transform solution can be attempted for Eqn.3.2 and the resulting O(x) values are the new y-coordinates of the function represented in plane I (Fig.3.1). It is possible that O(x) takes both positive and negative values and this poses a practical problem. Adding a uniform bias to make O(x) wholly positive is a way out. This also helps while recording the intensity pattern, since the low intensity regions of the signal are pushed beyond the non-linear 'toe' of the H - D curve of the photographic emulsion used, provided the larger intensity regions still remain in the linear range.

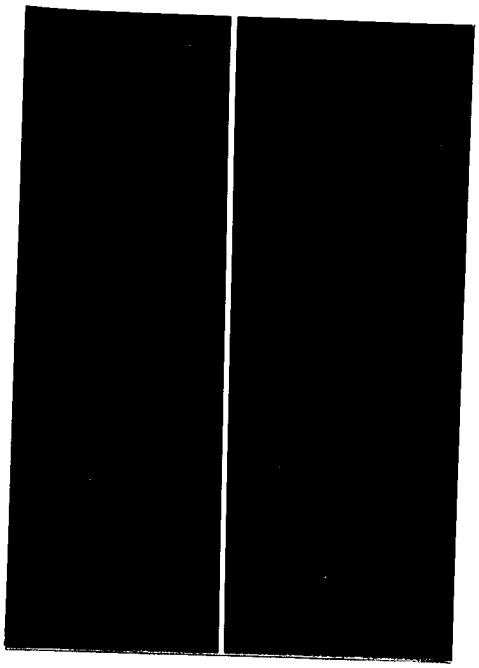

(a)

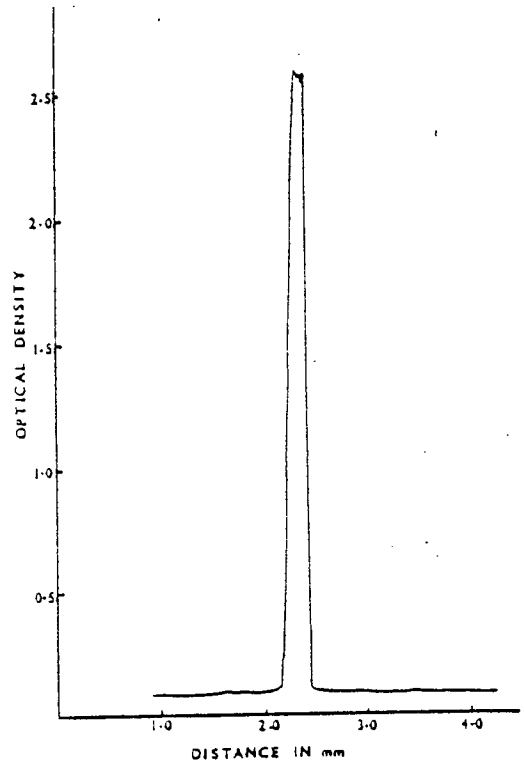

(b)

Fig.3.2(a) The central region of the cylindrical lens line spread function.

(b) Microdensitometer trace across the line spread function.

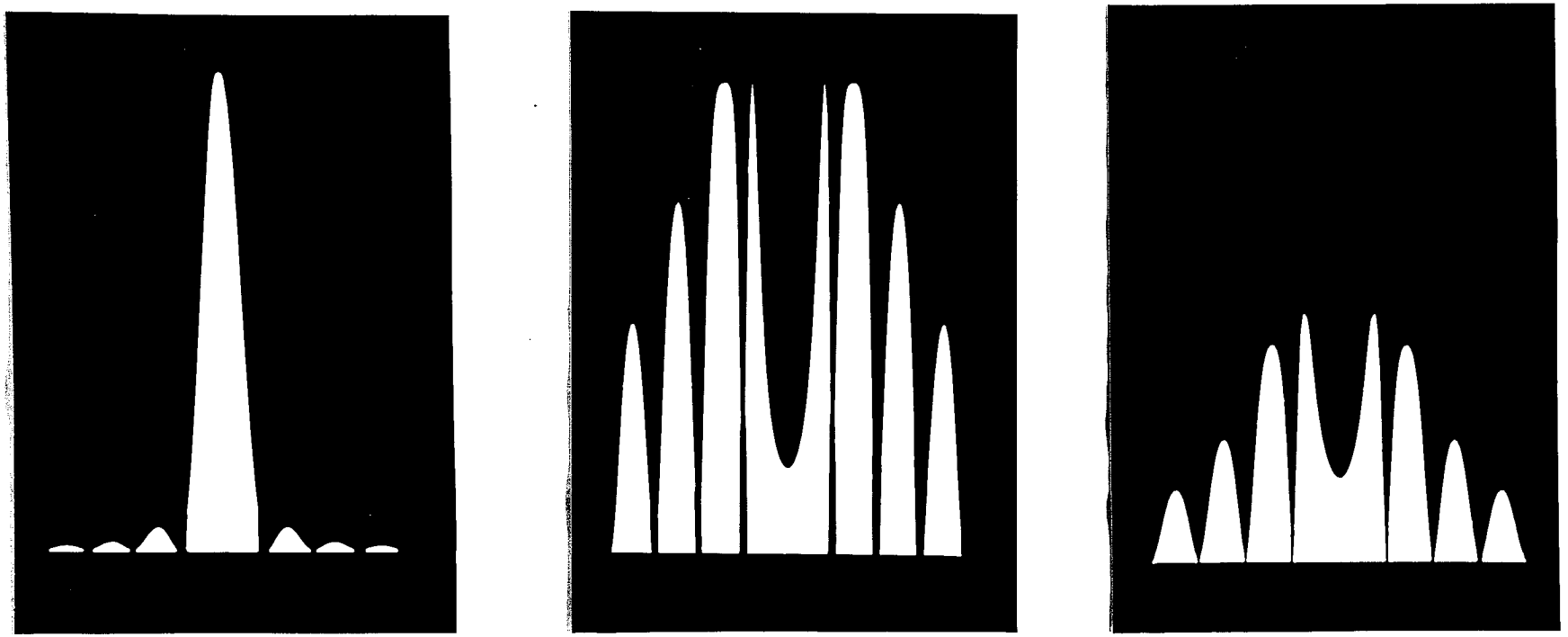

(a) (b) (c)

Fig.3.3. The binary input objects for the cylindrical lens imaging set-up shown in Fig.3.1; (a) $\varepsilon = 0.0$ (b) $\varepsilon = 0.05$ and (c) $\varepsilon = 0.1$

Fortunately we do not have to resort to such a complicated correction procedure, since the achromatic cylindrical lens we used has a sharp line spread function in the central region of the lens. The line spread function and a microdensitometer trace across it are shown in Fig. 3.2.

The black-and-white object I of Fig. 3.1 is made with the help of a computer plotter. The profile of the required function is drawn through the plotter and the area enclosed between the curve and X-axis is inked and the resulting pattern is photoreduced onto a high contrast film (e.g. Kodalith Ortho type 3 (2556)).

Corresponding to the poles of the function represented here it is noticed that the intensity at the output plane was not zero. This is because the functions are not well behaved at the poles and the steep rise on both sides of the poles results in a small amount of light being spread into the region of the poles. We have overcome this by, first, slightly smoothing the curves around the poles and second by enlarging the poles to either sides by a small amount.

Section 3.3. Intensity variations for different amplitude filters and the generation of filters by photographic recording of the intensity variations.

Three black-and-white objects are generated on Kodalith film. The first has a clear region between x-axis and $y = \left(\frac{\sin x}{x} \right)^2$ (Fig.3.3a) This is used as the input in the set-up shown in Fig.3.1 and the output intensity variation, proportional to $\left(\frac{\sin x}{x} \right)^2$, is recorded

with a photographic contrast index value (gamma) of one. The record has an amplitude transmittance proportional to $|x|/|Sinx|$ (which is the required amplitude transmittance variation of an inverse filter) provided we are in the linear range of characteristic curve of the emulsion. However, in this case we are well into the non-linear region of the curve at some places and hence we can only get an amplitude mask which approximates the modulus of the inverse filter function.

The second and third black-and-white objects are designed to give appropriate intensity variations for producing Wiener filters with noise ratio parameter(ε) equal to 0.05 and 0.1 respectively. Following the method described in the previous paragraph, for inverse filters, we can place profiles of $\left\{(H^2 + \varepsilon)/(H)\right\}^2$ (where $H = \frac{Sinx}{x}$) in front of the cylindrical lens and by recording the proportional intensity distribution in the output, with gamma equal to one we can get Wiener filters with amplitude transmittance proportional to $|H| / (H^2 + \varepsilon)$. But $\{(H^2 + \varepsilon) / |H|\}^2$ goes to infinity when sinx = o. So we have placed in front of the cylindrical lens $\{|H|/(H^2+\varepsilon)\}^2$ instead. (Fig. 3.3 b & c). This necessitates taking a print of the 'negative' filter obtained from the cylindrical lens.

In our case the middle region of the cylindrical lens where the line spread function is sharp, is long compared to the maximum value of y in the input profile. Hence a substantial region in the output plane has an intensity distribution proportional to the input profile. Great care was taken to align the y-axis (of the input function) parallel to the axis of the cylindrical lens.

The film we have used for recording the intensity pattern is SP348,

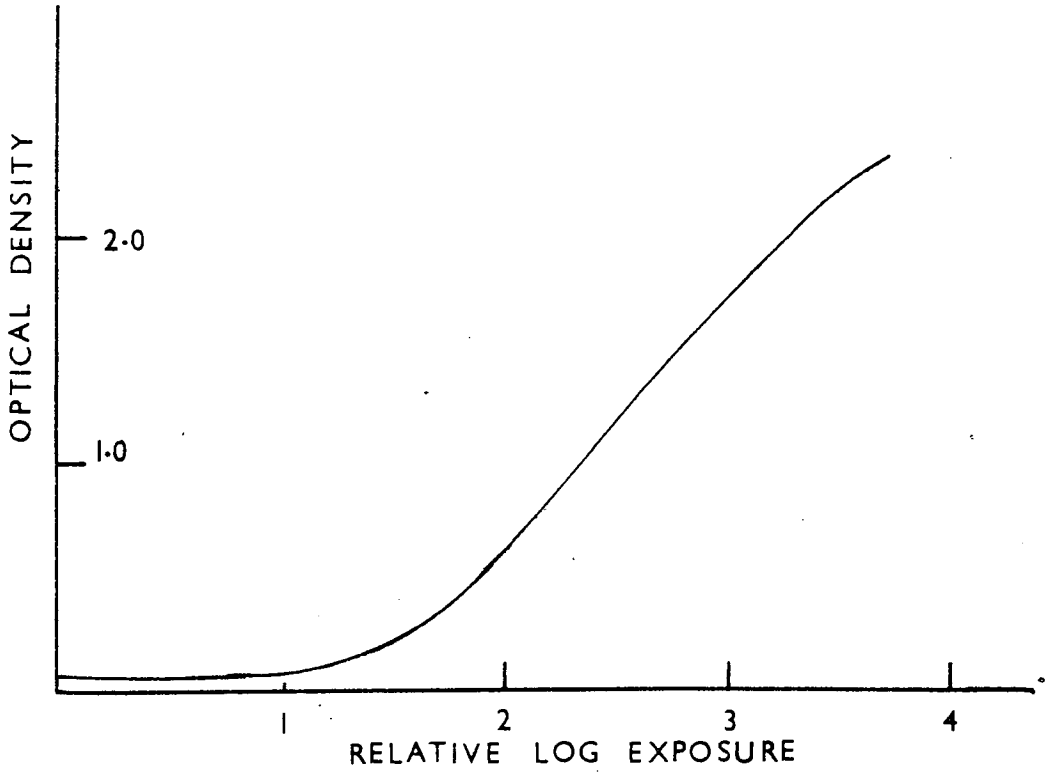

Fig.3.4. The calibration curve for Ilford Technical Orthochromatic film (SP348). The developer used is Ilford PQ universal at 1:9 concentration; development time is 3 mins.at 20°C. $\gamma \simeq 1$.

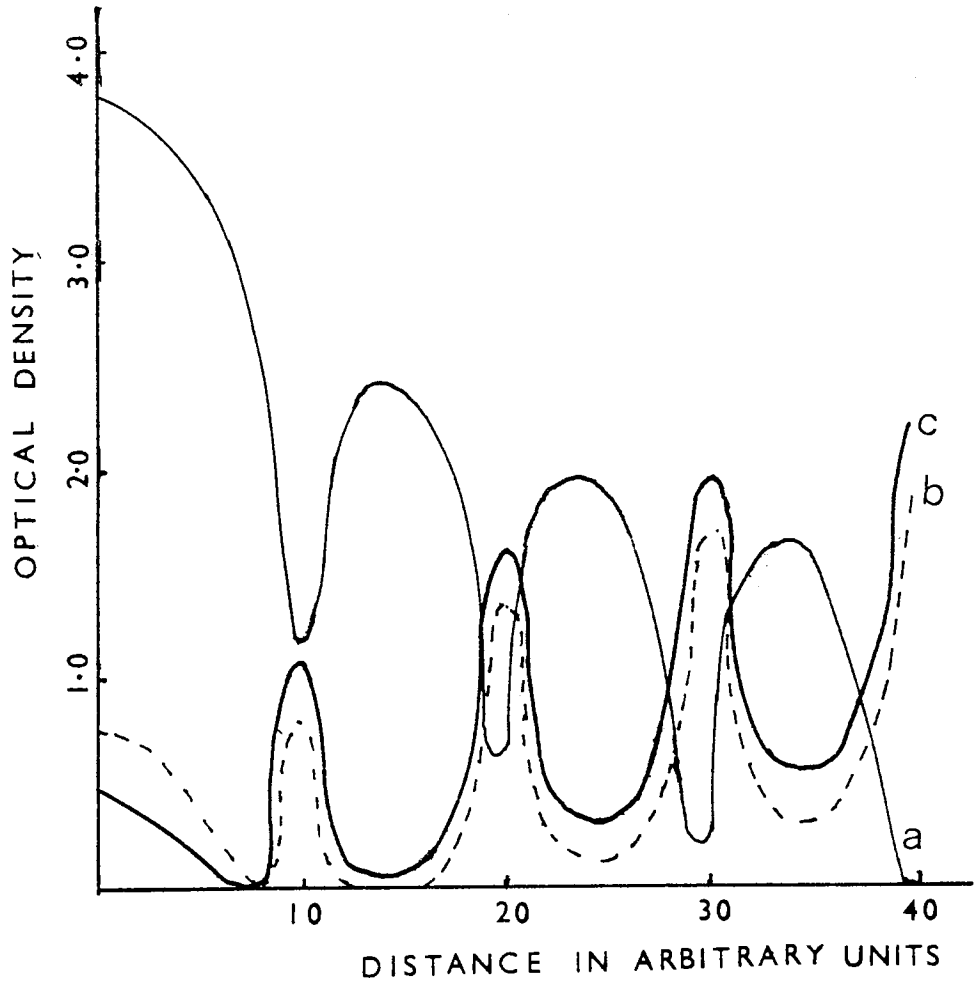

Fig.3.5 Graphs showing the density variations across the filter (calculated theoretically); (a) ε = 0.0 (b) ε = 0.05 and (c) ε = 0.1.

now called the Ilford Technical Orthochromatic. It is calibrated using a standard step-wedge and we have obtained a contrast of one approximately when developed for three minutes in Ilford 'P Q Universal' with 1:9 dilution at 20^{o}C. The calibration curve which is a plot of the intensity values in logarithmic scale, versus optical density, is shown in Fig.3.4.

(Alternatively, the film can be calibrated using the cylindrical lens. By placing a binary step function with known step-ratios in front of the cylindrical lens we obtain a range of intensity steps of known ratios. These steps are recorded and processed and the density values measured. Thus the H-D curve is plotted and the emulsion calibrated).

From the amplitude transmittance values of the inverse and Wiener filters, we calculated the corresponding optical densities. These densities are plotted in Fig.3.5. We excluded those points corresponding to H(x,y) = 0.0 which would result in completely transmitting and completely opaque regions in the inverse and Wiener filters respectively. From Fig.3.5 we see that for a filter with three side lobes, the density range for an inverse filter is from 0.0 to 3.8 while for Wiener filters (ε = 0.05 & 0.1) it is only from 0.0 to 2.3. Ilford SP348 emulsion for the development specified in the last but one paragraph has a linear range from 0.3 to 2.50. The film is prefogged, typically 2 - 3% of the main exposure, to push all the low density regions into the linear range (The high density regions in the Wiener filters still remain just within the linear range). So, excluding the points where

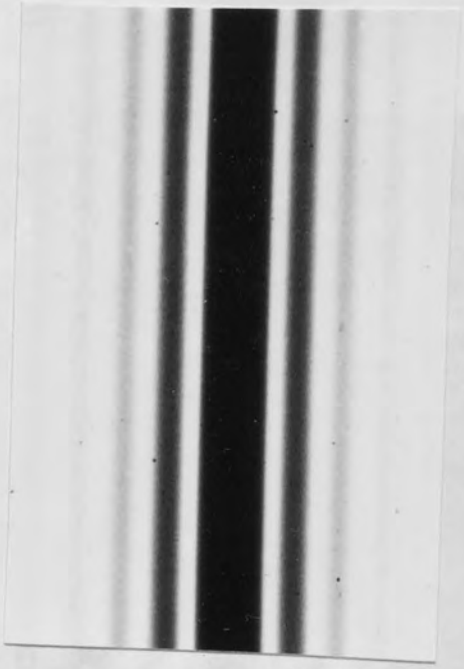

3.6(a)

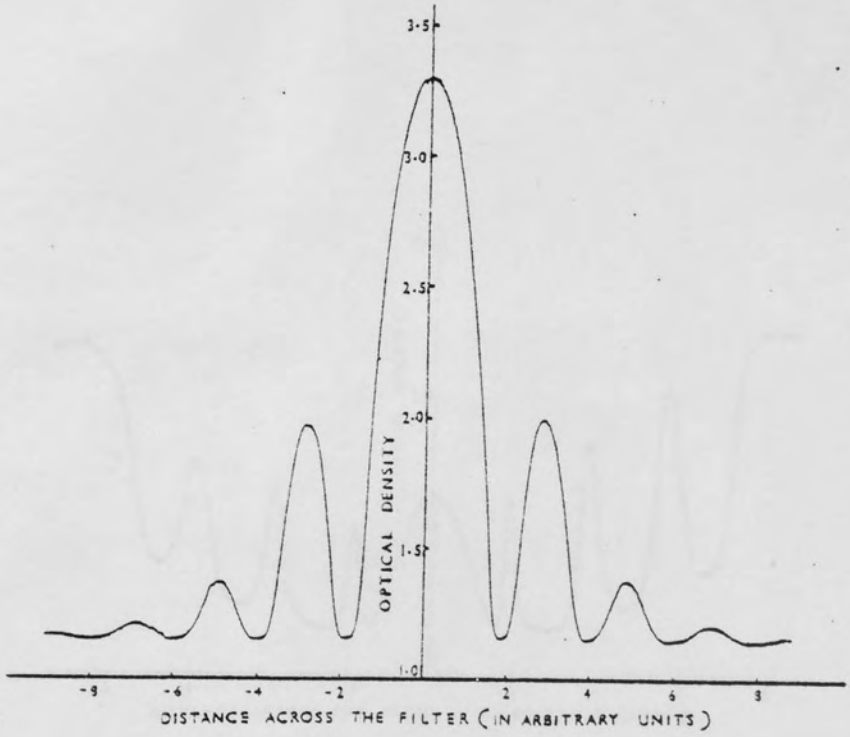

3.7(a)

Fig. 3.6(a) The photograph of the amplitude filter for linear motion blur ($\varepsilon = 0.0$).

Fig. 3.7(a) Microdensitometer trace across the filter shown in Fig.3.6(a).

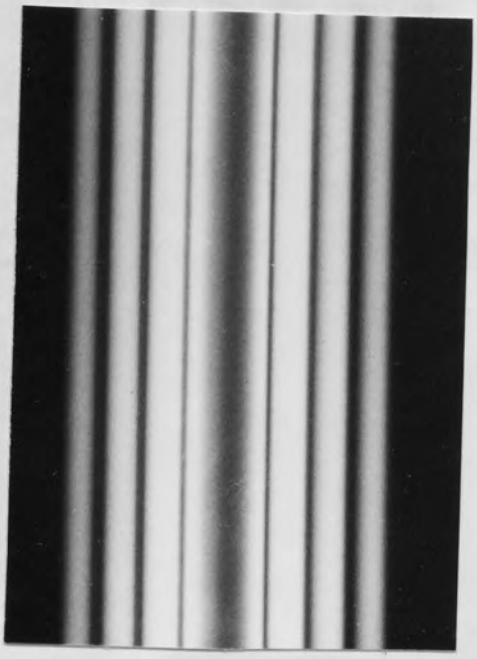

3.6(b)

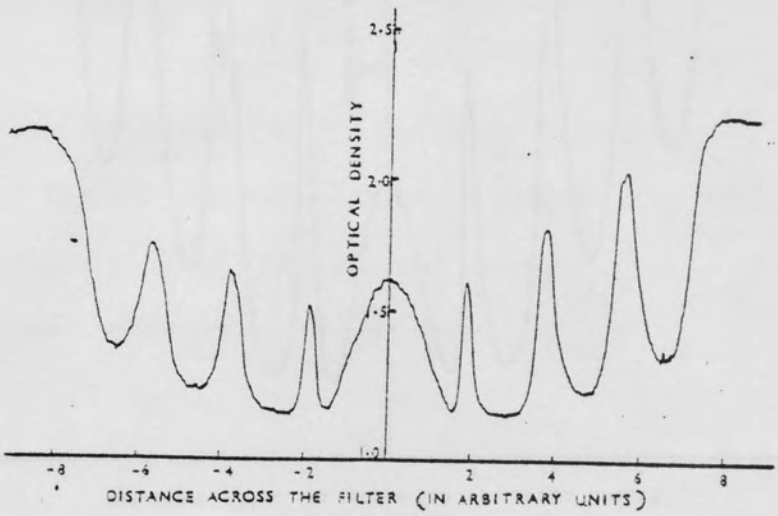

3.7(b)

Fig.3.6(b) The photograph of the amplitude filter for linear motion blur ($\varepsilon = 0.05$).

Fig.3.7(b) Microdensitometer trace across the filter shown in Fig.3.6(b).

3.6(c)

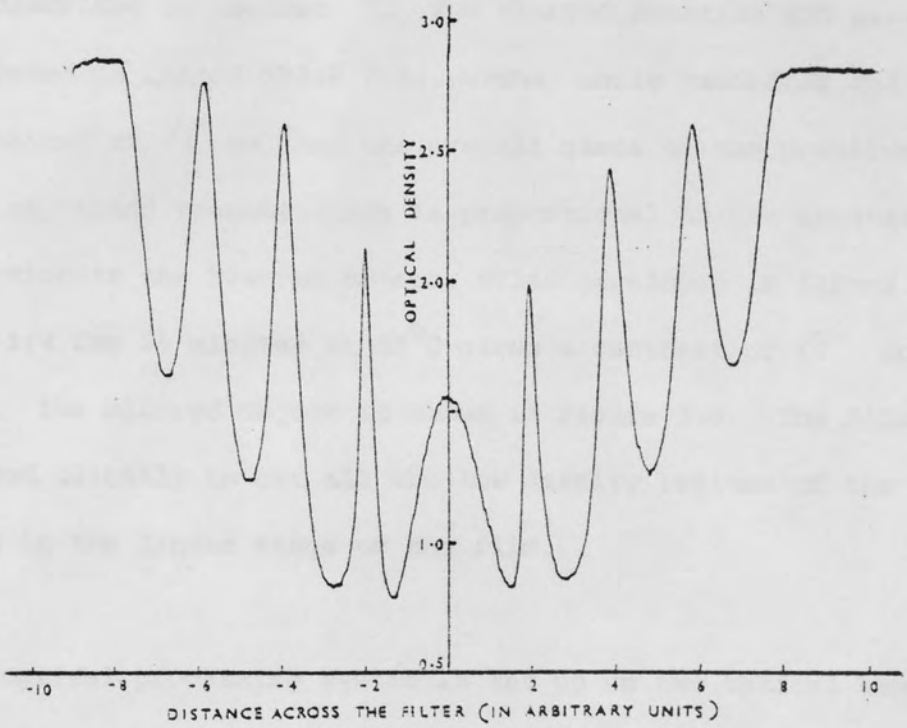

3.7(c)

Fig.3.6(c) The photograph of the amplitude filter for linear motion blur ($\varepsilon = 0.1$).

Fig.3.7(c) Microdensitometer trace across the filter shown in Fig.3.6(c).

$H(x,y) = 0.0$ and their immediate neighbourhood, we see that for the Wiener filters, we are just within the linear range of the film.

Amplitude filters are generated with $\varepsilon = 0.0$, 0.05 and 0.1. ($\varepsilon = 0.0$ gives an approximation to the $|x| / |\sin x|$ function). The filters produced are shown in Figure 3.6. Microdensitometer traces, taken across the filters are shown in Figure 3.7.

Section 3.4. Optical processing system and the deblurring experiment :

Linear motion blur is simulated in the laboratory, using the method described by Goodman [42]. The blurred negative and positive are recorded in Ilford SP348 film. Gamma, while recording and printing is maintained at $\sqrt{2}$ so that the overall gamma of the positive is 2 and its amplitude transmittance is proportional to the intensity distribution in the blurred object. SP348 developed in Ilford 'Phenisol' diluted 1:4 for 2¾ minutes at 20°C gives a contrast of $\sqrt{2}$ approximately. The blurred object is shown in Figure 3.8. The film is pre-fogged slightly to get all the low desnity regions of the object recorded in the linear range of the film.

An optical processing system is set up on two optical benches, each 2m long on vibration free mounts (polystyrene foam). (See Fig. 3.9 for a schematic representation). One carries the laser L, beam expander BE, a collimator C (a 178 mm lens) object I and a Fourier transforming lens L1. (A914mm aerial camera objective). The second bench carries an aerial camera of 914 mm focal length, the objective of which forms the second Fourier transforming lens (L2). The

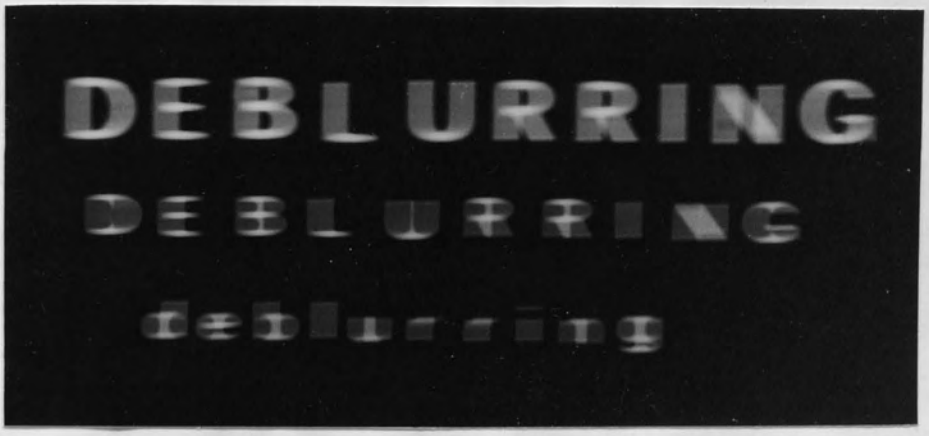

Fig.3.8. Object blurred due to linear motion of the camera.

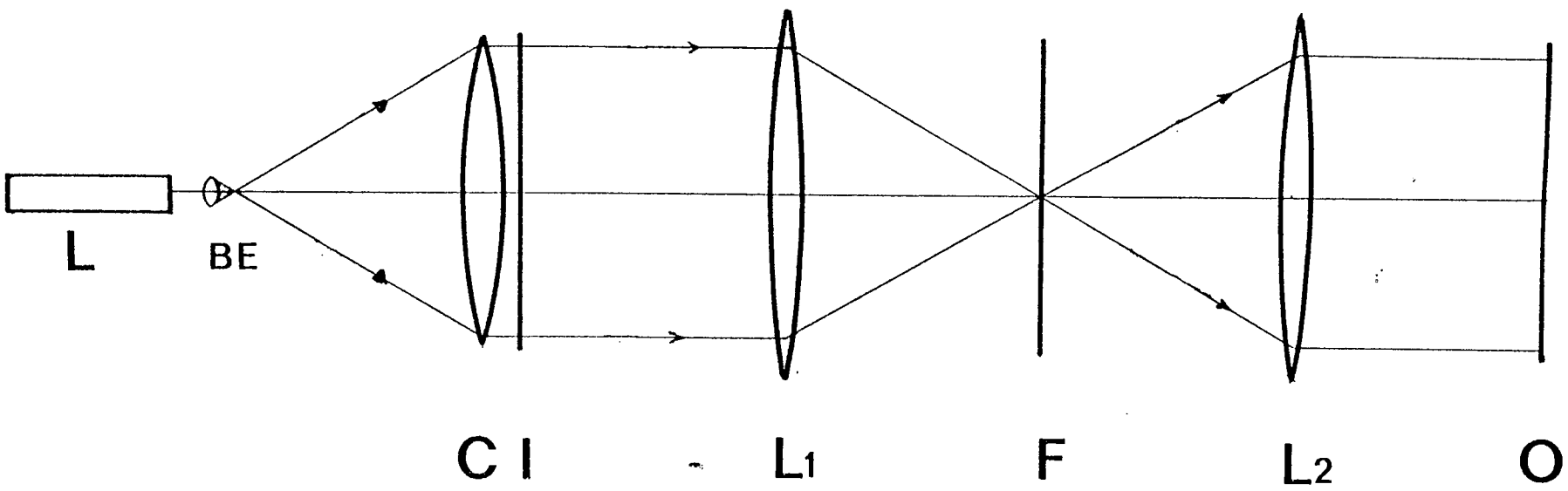

Fig. 3.9. The optical processing system: L Laser, BE Beam expander. C Collimator, L_1, L_2 Fourier Transforming Lenses, I Input plane, F Filter plane, and O Object plane.

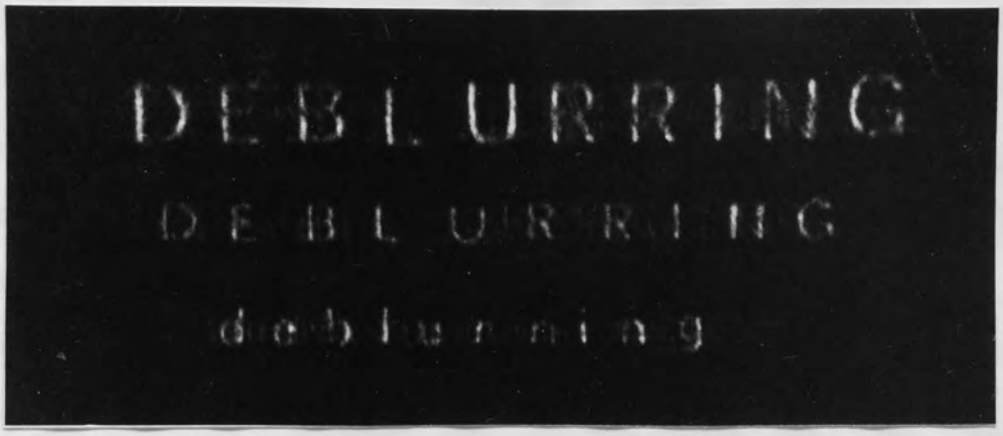

(a)

(b)

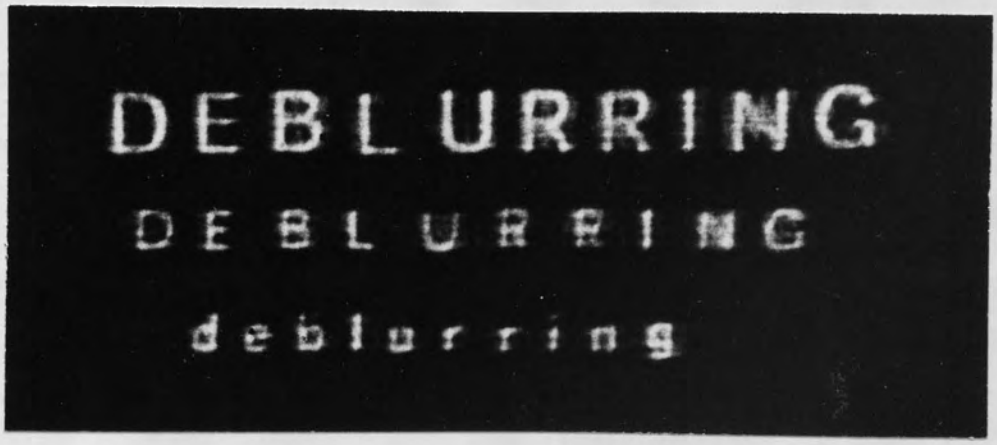

(c)

Fig. 3.10. The deblurred outputs obtained from the object shown in Fig.3.8.
(a) $\varepsilon = 0.0$ (b) $\varepsilon = 0.05$ and (c) $\varepsilon = 0.1$

blurred object, immersed in a cedarwood oil gate so that nonuniformities in the recording film are compensated is mounted at the first focal plane of the first Fourier transforming lens (L1). The lens L1 Fourier transforms the blurred object and the spectrum appears at its second focal plane (F). The distance between the two Fourier transforming lenses is so adjusted that the first focal plane of the first lens coincided with the second focal plane of the second lens and in this plane (F) we mounted the deblurring filter. The corrected spectrum is recombined by the lens L2 to form the deblurred output.

The object shown in Figure 3.8 is deblurred using sandwich filters formed between the phase filter, developed in Chapter 2, and different amplitude filters. The deblurred outputs are shown in Figure 3.10.

Section 3.5. Results and discussions.

The results shown in Figure 3.10 show a considerable improvement on the original blurred object of Figure 3.8. The spread in the horizontal direction, the direction of the blur and the contrast reversals suffered by the blurred object (especially noticeable in the second and third lines) are quite sufficiently rectified. (The contrast reversals in the blurred image are due to the negative regions in the blur transfer function).

With $\varepsilon = 0.0$, the deblurred output has invariably some noise in it. This is because the inverse filter is high frequency enhancing and the high frequency noise encountered in a coherent system (photographic grain noise, dust on lens surface etc) is amplified.

With $\varepsilon = 0.1$ the noise suppression is good but the resolution of the output is affected by the high frequency attenuation caused by the amplitude filter. The best result is produced with $\varepsilon = 0.05$ when most of the noise is suppressed with the object resolution not seriously affected.

Even though the deblurred outputs show a great deal of enhancement, we must point out that they never can be as good as the original object. This is due to the loss of information suffered at the poles of the blur transfer function and this information is not recovered by our processing. The physical size of the filter, which is limited by the dimensions of the lenses used in the processing system, imposes a limit on the space-bandwidth product of the filter. The highest frequency allowed through the filter may fall much below the 'cut-off' frequency of the Fourier transforming lenses and hence the filter can have a restricting influence on the ultimate resolution of the output, as well as the limit set by the optics involved in the processor.

C H A P T E R 4

THE AMPLITUDE FILTER FOR OUT-OF-FOCUS PICTURE CORRECTION

Section 4.1 Introduction

Here, as in the previous chapter, we develop the amplitude filter as a density variation on a photographic film. The cylindrical lens method of Chapter 3 suits very well when the blur transfer function is line symmetric. For defocusing, the blur transfer function is circular symmetric and here we have adapted the rotating disc method of Tsujiuchi[29] to generate an intensity variation proportional to the Wiener filter amplitude transmittance of the blur. This intensity variation is then converted into a proportional amplitude transmittance variation by photographic recording with a suitable gamma provided the recording is done entirely within the linear range of the film used. Since the blur transfer function for defocusing has a very large range, the intensity variation proportional to the Wiener filter amplitude transmittance also has a very large range falling well into the nonlinear regions of the film. So the filters generated here possess a certain amount of error introduced due to film nonlinearities and they are only approximate representations of the true Wiener filter amplitude transmittance.

We have attempted to correct the effect of film nonlinearity by employing a computer assisted method to generate the filter. We have made use of an image processing peripheral (known as the FR80) available at the Atlas computer Centre, Chilton (Oxfordshire) to

produce a predetermined intensity variation. Again, we were limited by the maximum intensity step available in the FR80 to produce the highest density value. As a result,the low transmittance regions of the filter suffer abrupt jumps in transmittance variation and the filter does not accurately represent the theoretical Wiener filter function. The details of the attempt are given in Section 4.2.

In Section 4.3 we have developed Wiener filters for circular blur using a slightly modified version of the method first described by Tsujiuchi (Miles[62] used a similar method to generate sinusoidal zone plates). In this section we have not tried to incorporate film non-linearity correction.

A few suggestions for eliminating the errors due to film nonlinearity while using the photo-mechanical method of Section 4.3 are given in Section 4.4. We have not tried to implement these suggestions.

The filters developed in Section 4.3 along with the phase filter of Chapter 2 are used to deblur out-of-focus pictures. The experimental results are discussed in Section 4.5.

Section 4.2. Quantized amplitude filter through computer aided design.

The image processing peripheral FR80 is capable of producing 256 intensity levels on its output screen. The complete plotting area has coordinates from 0 to 16383 in both directions, with separate

addressing capability for each of the coordinate points. Combined with a 35mm camera, each point (or raster unit) recorded has a width of 0.0000596". This high resolution in conjunction with the 256 level grey-scale help to produce an almost smooth representation of any continuous-tone amplitude transmittance variation that falls within the grey-scale range of the FR80.

For generating the Wiener filter the following procedure is adopted: Using all the 256 intensity levels an intensity step function is produced on the output screen. This step function is photographed onto Ilford HP4 film using the 35mm camera attached to the FR80. The film is developed in Ilford Phenisol (diluted 1:4) for 4 minutes at 20^{o}C. (We choose this developer and the development time, since this combination gives a wider range of densities for the available intensity variation). The optical density values of the various steps produced are measured accurately using a densitometer. The Wiener filter is then considered to be divided up into a finite number of annular regions and for each of these regions the average amplitude transmittance is calculated theoretically. These amplitude transmittance values are then converted into the corresponding optical density values. By comparing these density values with the densities generated in the previous calibration stage we have determined within a certain degree of approximation the intensity steps which would produce the various density levels. Finally, the filter is generated by drawing annular regions of these various intensities, starting from the smallest circle that can be drawn using the FR80 to the largest one giving the periphery of the filter. This circular intensity pattern is photographed onto Ilford HP4 using exactly the same processing as

Fig.4.1. The Wiener filter generated by using the FR80. Transmittance variation in steps is noticeable.

before. Fig.4.1 is a photograph of the Wiener filter thus generated.

One of the main advantages of this method is that we are not dependent on the relation A (amplitude transmittance) = $I_o^{-\gamma/2}$ (I_o is the input intensity variation) for generating the amplitude transmittances. Hence, we have the freedom to use the complete range of the H - D curve of the emulsion without involving the errors the film nonlinearities would otherwise produce.

The filter produced is essentially a quantized version of a continuous transmittance variation. Though each annular width in the filter is considerably small compared to the overall diameter of the filter, quantization still introduces a certain amount of error. (The ratio of the annular width to the diameter of the filter is about 1.28×10^{-4}). Moreover, the FR80 can only draw circles of certain finite radius and beyond and hence a small circular area around the centre of the filter had to be of uniform amplitude transmittance representing the average for that region.

Finally, we come to the greatest draw-back of this method which has actually prompted us to abandon the method altogether. We were not able to generate a wide enough density range to accommodate all the density values in the filter using the 256 intensity levels available in the FR80. We have used films of different speeds and ranges and also tried various processing methods, but the range of densities we could get was only 1·55 (from 0.05 to 1.6). (The filter has a density range of about 4, excluding the immediate neighbourhood of the roots of the Wiener filter function.)

Fig.4.2. The binary input sector for the imaging set-up shown in Fig.4.3.

We have tried to generate higher densities by repeated drawing of the same regions a few times over, with the highest intensity level. This has resulted in spreading of intensity to neighbouring regions. We understand that the intensity range in the 256 intensity levels can be enhanced by changing the hardware of the system; but that was something beyond our control. However, if such an enhanced intensity range is made available the above described method can produce the amplitude filters utilizing both the linear and nonlinear range of the photographic film.

Section 4.3

The photomechanical method for continuous tone filters without compensating for film nonlinearities.

A carefully calculated and fabricated sector as shown in Fig.4.2 consisting of transmitting areas in opaque background is rotated using a motor. When a lens system is used to image the rotating sector, with the optical axis of the system coinciding with the axis of rotation of the input pattern, then on the image plane we obtain a circular-symmetric intensity variation. The nature of the intensity variation is obviously determined by the design of the input sector. The input pattern drawn using polar coordinates has the area enclosed between the curve $\theta = f(r)$ and the line $\theta = 0$ fully transmitting. If θ is proportional to the Wiener filter amplitude transmittance $H(\propto |J_1(r)/r| / [(J_1(r)/r)^2 + \varepsilon])$ with r being the distance from the centre of the filter, then the circular intensity pattern generated at the output plane of the imaging lens will be proportional to the Wiener filter amplitude transmittance. Finally, photographic recording of

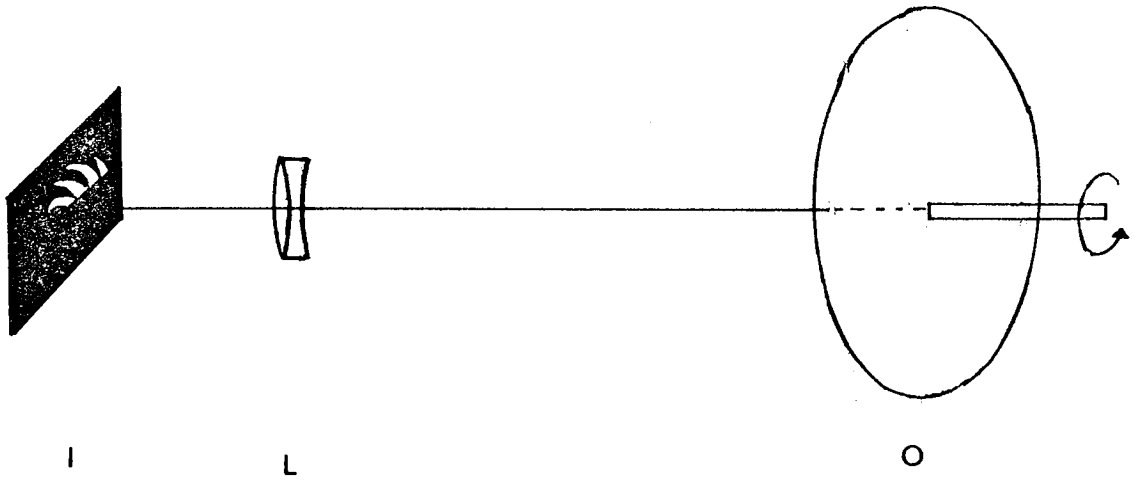

Fig. 4.3. The experimental set-up for generating the circular symmetric master amplitude filter. The binary pattern at input I is projected by the lens L onto a rotating film at O.

this intensity variation with an appropriate gamma, gives the amplitude part of the Wiener filter.

In practice, setting up of an imaging system with a transilluminated rotating object as the input can be quite difficult. In our work here we have used a stationary input which was projected using an enlarger onto a rotating film(Fig.4.3). The film which was mounted on a motor (that was checked for vibration and wobbling) was accurately adjusted so that the centre of rotation coincided exactly with the centre of the pattern that was projected onto the film. The filter thus produced is an enlarged version and is photoreduced to the required size using a well corrected camera. The overall gamma of the final record is kept at two approximately, so that within the linear range of the film the final amplitude transmittance is proportional to the intensity variation recorded in the first step.

Section 4.4.

Some suggestions towards overcoming the errors due to nonlinear recording.

The computer-aided design of filters described in Section 4.2 has the potential for eliminating the nonlinearities introduced by the film, though in the process a quantized version of what should have been a continuous-tone filter results.In the previous section we have generated continuous-tone filters by imaging a transilluminated rotating object, wherein it is assumed that the intensity variation generated is converted into a density variation in the linear region of the recording film used.

Unfortunately this condition is not satisfied, since the intensity variation generated for the Wiener filter occupies the entire span of the H- D curve, low intensity levels falling in the "toe" region and the high intensity levels going well into the "shoulder" region of the curve. Hence, the amplitude transmittance of the filter generated will be only an approximation of the theoretical Wiener filter function. The following are some suggestions towards offsetting the problem of nonlinear recording when using the optical system of Section 4.3.

An obvious and easy way of minimizing nonlinear recording is to reduce the range of the filter function ($|G|$) by splitting it into two parts each having a transmittance proportional to $|G|^{1/2}$. Then each component is recorded separately on slightly pre-fogged film so that the low intensity regions in the filter are pushed beyond the "toe" region of the H - D curve.(We have actually applied this technique in the experiments described in Chapter 5.)

Another method of compensating for the logarithmic response of the film is by determining the H - D curve of the emulsion for the particular process used. This is done by recording a series of intensity steps of known intensity values and determining exactly the density values generated. The nature of the curve is determined by fitting an equation into the experimentally arrived at curve. This equation is made use of while calculating the input sector of Section 4.3.

An optical analogy of the computer assisted method of Section 4.2 is yet another way of compensating nonlinear errors. First of all

we generate an input pattern for the photomechanical set-up which gives a series of annular intensity steps of known step-ratios. This intensity pattern is then recorded on the same type of emulsion to be used for recording the filter and the various density values are accurately measured. From these measurements a relationship is established between the product of the input openings (or arc-lengths)and their distances from the centre of rotation of the pattern and the corresponding density values generated. The densities to be generated are calculated from the theoretical amplitude transmittance values. Finally, the input binary pattern is designed by comparing these theoretical density values with those generated by the intensity steps.

This method requires that during the calibration stage and while actually recording the filter the internal f/number of the optical system used should remain the same.

The last two methods mentioned above involve intermediate density measurements and hence the accuracy of the method is dependent on how well we can measure the densities. As we go into the higher density regions the measuring accuracy of the densitometer decreases. This is a major limitation on the exactness of the filters produced.

Section 4.5

Deblurring experiment, results and discussion.

We have produced, using the method described in Section 4.3, amplitude filters for enhancing out-of-focus pictures. We have not

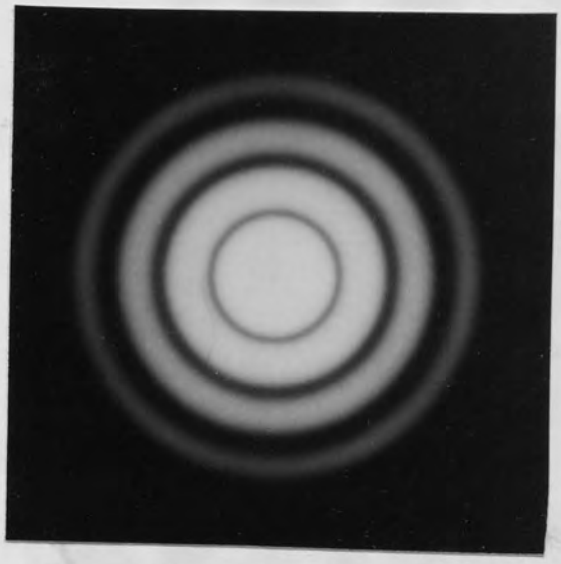

4.4(a)

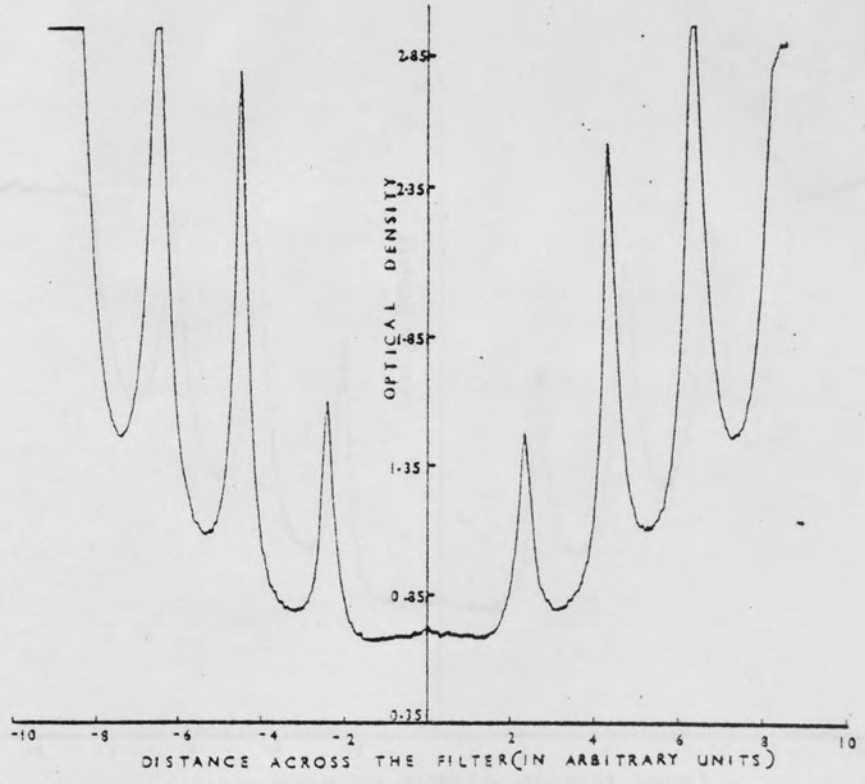

4.5(a)

Fig.4.4(a) A Photograph of the amplitude filter generated ($\varepsilon = 0.05$)

Fig.4.5(a) Microdensitometer trace through the filter shown in Fig.4.4(a).

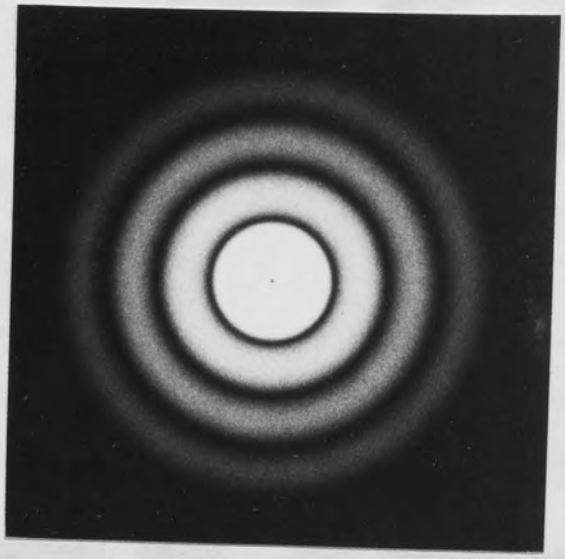

4.4(b)

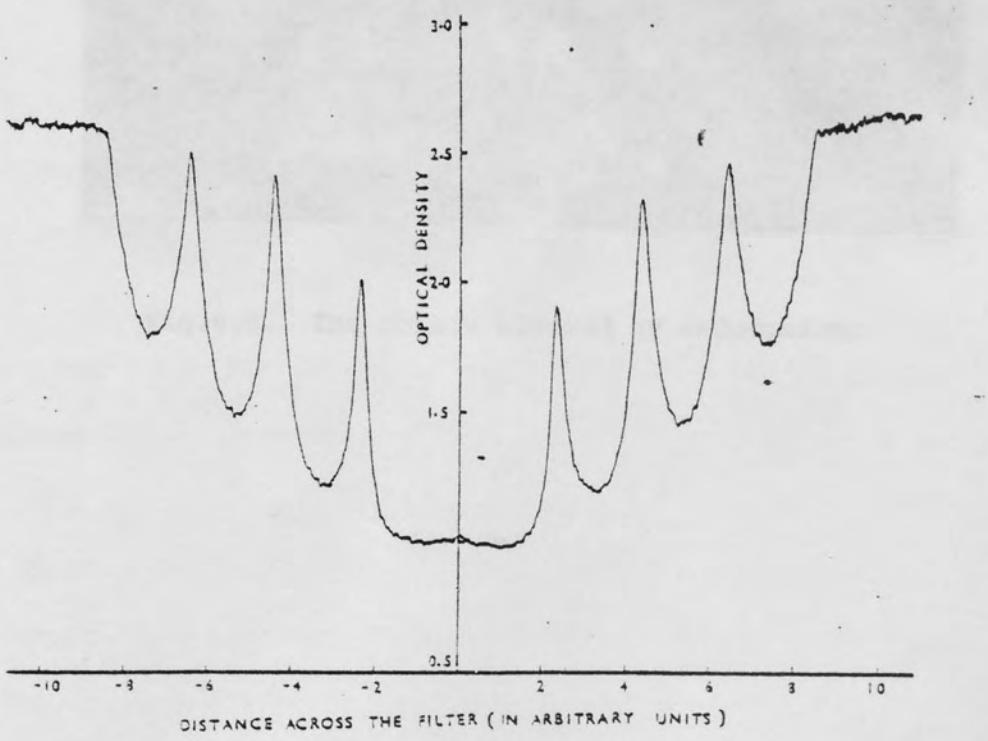

4.5(b)

Fig.4.4(b) A Photograph of the amplitude filter generated (ε = 0.1)

Fig.4.5(b) Microdensitometer trace through the filter shown in Fig.4.4(b).

Fig.4.6. The object blurred by defocusing.

tried to correct nonlinear recording. The input binary pattern of Fig.4.2 was made on a high contrast film. Two binary input patterns were generated which produced intensity variations proportional to $|H|/(H^2 + \varepsilon)$ with ε, the noise to signal power - spectral ratio equal to 0.05 and 0.1 ($H = J_1(r)/r$). Ilford Technical Orthochromatic film was used to record the intensity variations. The gamma was maintained at $\sqrt{2}$.

Enlarged versions of the filters obtained from the projector were reduced to proper size, again on Ilford Technical Orthochromatic film with gamma kept at $\sqrt{2}$. The overall gamma of the 'positive' is 2 and the amplitude transmittance of the filter is proportional to $|H|/(H^2 + \varepsilon)$ within the linear range of the H - D curve of the film used. The filters are shown in Fig.4.4. Fig.4.5 showing microdensitometer traces across the filter gives an idea of the density variations in the filters.

The out-of-focus picture shown in Fig.4.6 is first deblurred with only the phase filter developed in Chapter 2. The result is shown in Fig.4.7a. The optical processing system used is the same as that described in Chapter 3. Then the amplitude filters developed in this chapter are combined with the phase filter to deblur the same object. The deblurred outputs are shown in Fig.4.7b & c.

Fig. 4.7a shows that the contrast inversions realized by the phase filter are very satisfactory. The results of complex filtering point to the fact that the introduction of the amplitude filters, which are only approximations, creates more problems than solving them.

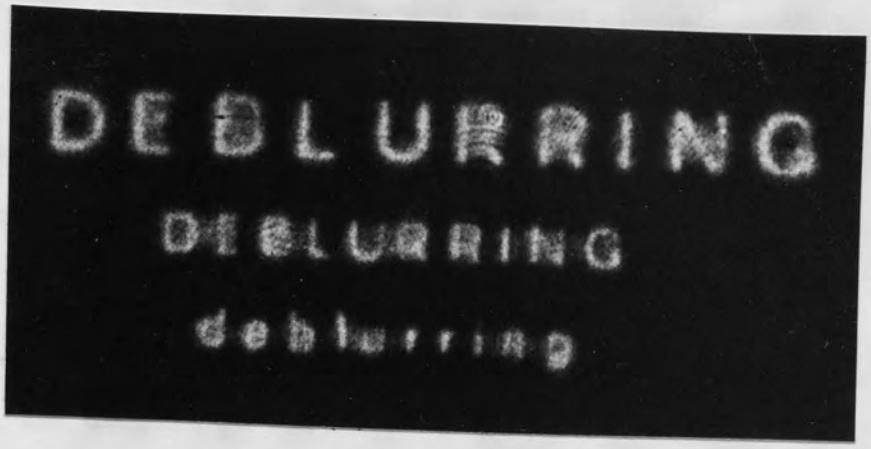

(b)

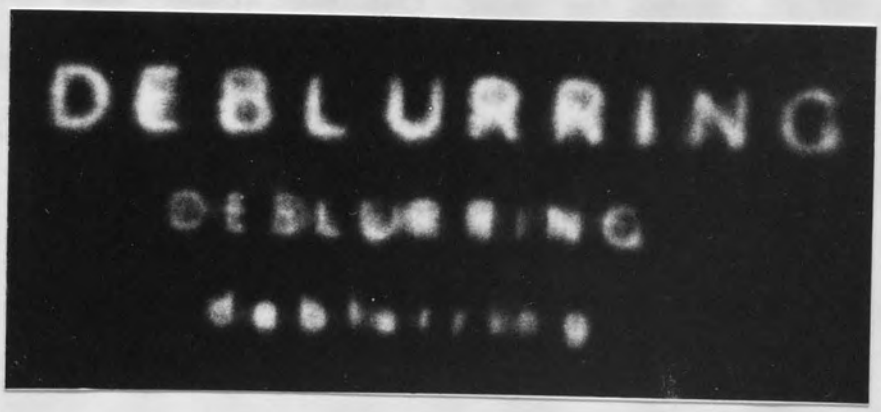

(c)

Fig.4.7. The deblurred outputs from Fig.4.6.
(a) using the phase filter alone.
(b) using sandwich filter with ε = 0.05.
(c) using sandwich filter with ε = 0.1.

Still comparing the results of Fig.4.7b & c carefully, we see that there is a fall in resolution as we increase the value of ε from 0.05 to 0.1. Though there is an overall improvement, the outputs here are not as well deconvolved as those shown in Chapter 3 for linear motion blur.

We believe, the drop in performance in the case of circular blur is due to the following reasons: (i) The blur transfer function for circular blur $(J_1(r)/r)$ has a much larger range than the sinc function which is the transfer function for linear motion blur. Consequently errors due to nonlinear recording are enhanced for circular deblurring filter. (ii) Since linear motion blur is one-dimensional the correcting filter has a fair amount of built-in redundancy while the filter for circular blur has no redundancy at all. As a result, blemishes in the filter will have a greater effect on the reconstructions in the case of circular blur than the one-dimensional blur.

We notice the same sort of deterioration in the quality of the outputs for circular blur while using binary hologram filters for deblurring, in Chapter 6.

C H A P T E R 5

DEBLURRING WITH A POSITIVE ONLY FILTER AFTER FURTHER BLURRING

Chapter 5.

Section 5.1. Introduction.

In the previous chapters we have discussed at length a method of deblurring both motion blurred and out-of-focus objects. Since these blurs are characterized by transfer functions having both positive and negative regions, the deblurring filters are made, for convenience, as a combination of an amplitude modulating part and a phase modulating part. However, there do exist certain other types of blurs which have wholly positive transfer functions. (Gaussian blur and triangular blur are two examples of blurs with positive only transfer functions). Consequently, the deblurring filters for these blurs are purely attenuating masks having only positive amplitude transmittances.

It is obvious that if the blur function of an input picture is known, by submitting the same picture to a further, exactly equivalent blur, the resultant picture will have the autoconvolution of the original blur as its final blur function. If the original blur function is either centre-symmetric (in the case of 2-d blur function) or line symmetric (in the case of 1-d function), for the new picture, the error in the Fourier plane (or the blur transfer function) is given by a wholly positive function. (The Fourier transform of the autoconvolution, here, is the product of two real functions and must be positive). So by subjecting a singly blurred picture to a second blur, the need for a phase filter is eliminated.

We, in this chapter, describe how a linear motion blurred object is deblurred using a 'positive only' filter. The main

problem with this technique is that, since the new blur transfer function is the product of two individual transfer functions, the dynamic range of the film, recording the deblurring filter, is much increased with consequent problems with the non-linearity of the photographic process. We have, however, managed to overcome this difficulty by building up the filter from a succession of photographic films, each processed to the correct fraction of the required function. The main problem now becomes noise, which must be met by a corresponding adjustment of ε in the Wiener filter employed.

Section 5.2 Theory

A blurred picture, g(x,y) of an original object scene, f(x,y) is given by

$$g(x,y) = f(x,y) * h(x,y) \quad \ldots\ldots\ldots\ldots\ldots \quad (5.1)$$

where h(x,y) is the impulse response of the blur and * denotes convolution.

For linear motion blur of the camera, h(x,y) is given by a rectangular function defined as

$$\begin{aligned} \text{rect } (x/a) &= 1 \text{ for } |x| < a/2 \\ &= 0 \text{ otherwise} \end{aligned} \quad \ldots\ldots\ldots\ldots\ldots (5.2)$$

Suppose we subject the blurred picture to another blur of exactly rect(x/a). The resultant doubly blurred picture is given by

$$\begin{aligned} g'(x,y) &= g(x,y) * \text{rect } (x/a) \\ &= f(x,y) * \text{rect } (x/a) * \text{rect } (x/a) \\ &= f * \Lambda (x/a) \quad \ldots\ldots\ldots\ldots\ldots (5.3) \end{aligned}$$

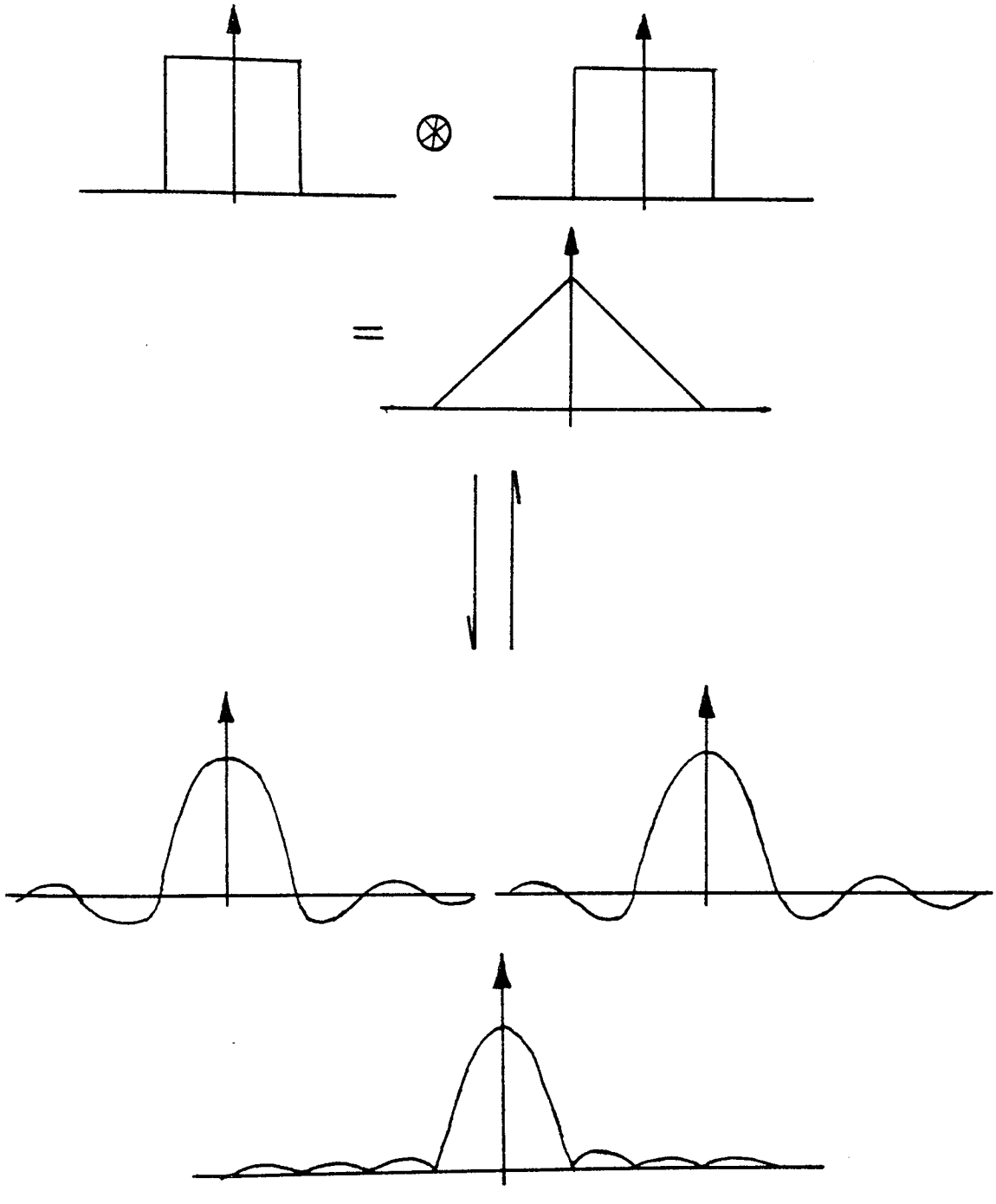

Fig.5.1. Diagrams illustrating the principle behind 'Positive only' filtering. The convolution of two blur functions (here rectangular function) in the object plane is equivalent to the product of their respective transfer functions in the frequency plane.

where $\Lambda(x/a) = 0$ for $|x| > a$

$= 1 - \left|\frac{x}{a}\right|$ for $|x| < a$ ..... (5.4)

By taking the Fourier transform of Equation 5.3 we obtain

$$G'(v_x, v_y) = F(v_x, v_y)\ H(v_x) \quad \text{..... (5.5)}$$

where G', F and H are the Fourier transforms of g', f and Λ respectively.

In particular $H(v_x) = \frac{\sin v_x}{v_x} \cdot \frac{\sin v_x}{v_x}$

(see Figure 5.1) which is a non-negative function.

From Equation 5.5 we recover F by passing G' through a Wiener filter [20]. The corrected spectrum is again Fourier transformed to form the deblurred picture.

Section 5.3 Development of the Wiener deblurring filter.

The Wiener filter, which is 1-d in our case is prepared using the cylindrical lens technique described in Chapter 3. The set-up shown in Figure 3.1 is used. The black-and-white object $f(x)^2$ has $f(x) = H/(H^2 + \varepsilon)$ with $H = \left\{\frac{\sin x}{x}\right\}^2$ (the new blur transfer function) and $\varepsilon = 0.05$. The resultant image whose intensity is proportional to $f(x)^2$ is recorded and printed on films developed to give gamma equal to one in both the steps. The print should ideally have an amplitude transmittance proportional to $\frac{H}{H^2 + \varepsilon}$ if the whole recording is done in the linear range of the film. Here, $f(x)^2$ has a very large

Fig.5.2. A linear motion blurred object.

Fig.5.3. The object shown in Fig.5.2 after undergoing a further blur of the same amount.

intensity range and we are well into the non-linear regions of the H-D curve of the film used.

We overcome this difficulty by building up the filter as a sandwich of three components, each having a transmittance proportional to $\left(\frac{H}{H^2 + \varepsilon}\right)^{1/3}$. Because of this split-up the intensity range involved are significantly smaller and we are in the linear range of the film except for smaller regions around the poles of the blur transfer function.

Section 5.4. Experimental

The linear motion blurred object is prepared in the laboratory using a shadowing technique described by Goodman[42]. The blurred object intensity variation is recorded on Ilford SP348 film which is developed in Ilford PQ Universal (diluted 1:9) for three minutes at 20°C, to give a gamma of 1 approximately. A print is made from this negative, again onto SP348, with the same development specified above so that the overall gamma of the print is 1. The blurred positive which is shown in Figure 5.2 is blurred again by exactly the same amount. The object after the second blur is shown in Fig.5.3. Doubly blurred negatives and positives are prepared on Ilford SP348 film, developed at each stage, to give a gamma of $\sqrt{2}$ approximately so that the overall gamma of the print is 2. (For a gamma of $\sqrt{2}$ SP348 was developed in Ilford Phenisol, diluted 1:4 for 2¾ minutes at 20°C).

The components which build-up the Wiener filter are also made

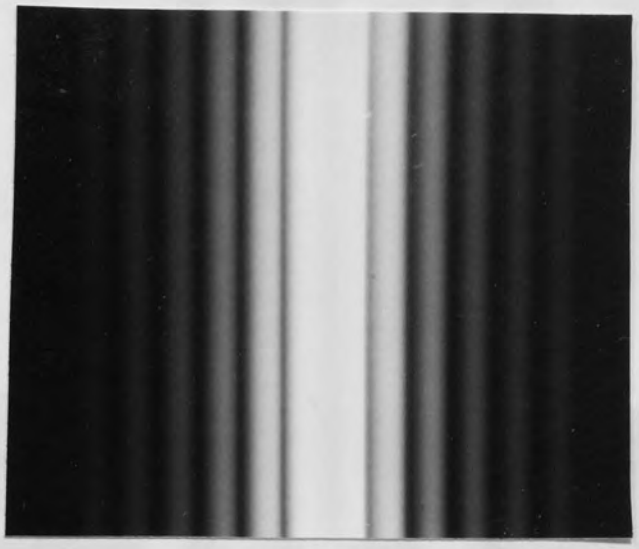

(a)

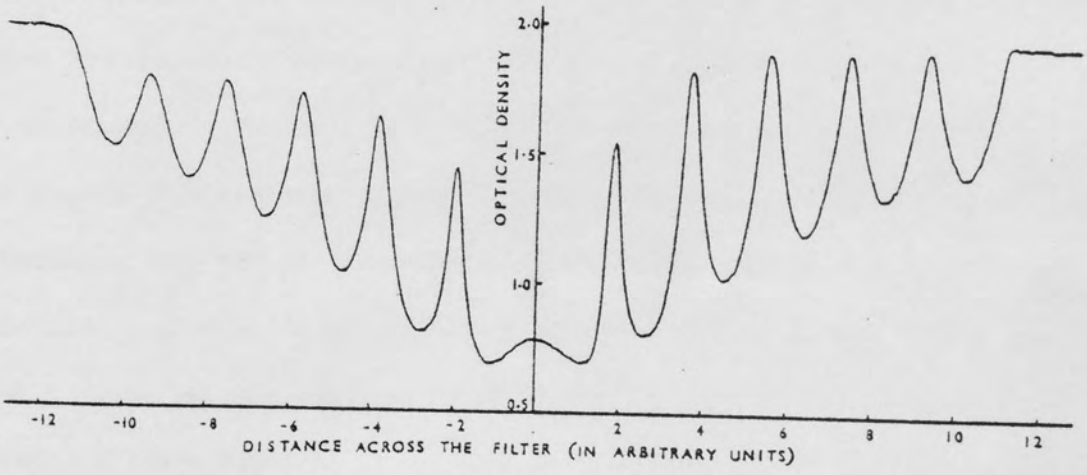

(b)

Fig.5.4. The filter containing a cube-root of the necessary Wiener filter transmittance.
(a) a photograph. (b) microdensitometer trace.

Fig.5.5. The deblurred output from Fig.5.3 after 'positive only' filtering.

on SP348, this time with gamma equal to one. Figure 5.4a shows one part of the Wiener filter with amplitude transmittance proportional to $\left\{ |H|/(H^2 + \varepsilon) \right\}^{1/3}$. Figure 5.4b is a micro-densitometer trace across the filter.

The optical processing system used is the same as that described in Chapter 3 (section 3.4). Here in the absence of a diffracting phase element the deblurred output is produced on-axis. The doubly blurred object is deblurred using the Wiener filter built-up as a combination of three component elements, each having an amplitude transmittance proportional to the cube-root of the necessary Wiener filter transmittance. The deblurred output is shown in Figure 5.5.

Section 5.5. Results and Discussion

Examining the doubly blurred object shown in Figure 5.3 we see that the contrast reversals noticeable in Fig.5.2 are somewhat compensated. This is as expected, since the contrast reversals of Figure 5.2 are due to the negative regions of the blur transfer function, and the blur transfer function of Figure 5.3 is wholly positive. The vertical lines of Figure 5.3 are rather badly spread out because of the extreme high frequency attenuation caused by the combined blur function.

The corrected picture shown in Figure 5.5 is a considerable improvement upon the blurred object of Figure 5.2. However, we notice that the Wiener filter is not able to rectify completely

the horizontal spread suffered by the letters. We believe that it is due to the following reasons:

The preparation of the doubly blurred object involves four photographic steps, including two contact printings. In each of the photographic steps involved one is bound to lose, at least, some information in spite of all the efforts towards proper exposure, linear recording etc. So the final blurred object has suffered a cumulative loss of information, which in turn affects the quality of reconstruction.

The filter function generated here, though made up of three parts, still does not represent the theoretical filter function quite accurately because of non-linear recording at some regions. (This is so because of the high contrast nature of the final blur function). Sandwiching of the three pieces together requires great care and precision since even a small amount of misalignment can seriously affect the quality of the output. Finally, the three films together introduce a considerable degree of phase distortion at the Fourier plane which causes some amount of spurious noise in the output.

CHAPTER 6

BINARY HOLOGRAMS : AN ANALYSIS AND THEIR APPLICATIONS FOR IMAGE-DEBLURRING

Chapter 6.

Section 6.1. Introduction

Computer-generated holograms (CGH) are a commonly used tool to generate a wide range of complex functions. The flexibility of these holograms has been utilized for adapting optical systems for both linear and nonlinear processing. Image deblurring[46] matched filtering[53] and realization of mathematical operations like differentiation[54] are some of the many uses of CGHs. In the case of image enhancement CGHs offer a new technique for realizing deblurring filters where the impulse response of the blur is not physically realizable. Such an extension of the physical process achieved by the new role of the computer as an imaging element is, by far, the most fruitful aspect of computer holography. We here confine ourselves to Fourier transform holograms of only two levels of amplitude transmittance (i.e. the binary type).

Since our aim is mainly the utilization of holographic filters for Fourier plane filtering, restriction to Fourier transform holograms is justified. We are prompted to the second restriction (namely, the binary amplitude transmittance) because of the easiness of fabrication of binary holograms.

Computer generation of holograms involves two major steps. First, we make a mathematical model of the object (or wavefront) to be generated (In our case, the object in the shape of a Fourier transform is either available as a mathematically defined function, or evaluated numerically from the known impulse response). Second,

by some means, the wavefront (which is in general complex) is displayed and recorded in such a way that the record acts like an optical hologram and reconstructs the original wavefront on illumination with a 'reference' wave. Before going into various ways of generating binary Fourier transform holograms, by computer, we give, in the rest of this section, a brief account of a few other methods of producing computer holograms.

Section 2 contains a brief description of various ways of generating binary Fourier transform holograms. Because computer-generated holograms are essentially digital, the reconstructions are always affected by sampling rate limitations and quantization errors in the hologram. These are discussed in Section 3. Section 4 describes ways of producing deblurring filters as binary holograms. Experiments utilizing binary holograms for deblurring are described in Section 5. There we suggest a method of overcoming the loss of resolution in the deblurred pictures due to coarse quantization levels in the binary filter. Finally we show the result of deblurring large objects with a binary hologram that is heterodyned to a high space-bandwidth product.

After having calculated the amplitude and phase of the light-wave distribution in the hologram plane, one of the most straight forward methods of recording the wavefront is by generating two transparencies, one having a density variation representing the amplitude of the wave and the other having a thickness variation proportional to the phase of the wavefront. The first transparency is easily made using a display-recording device with grey-level

capabilities. Careful exposure and controlled development produce the required density variation on a photographic plate. The second transparency is produced by photographing an intensity variation proportional to the phase of the wavefront to be generated and subsequently bleaching the record to form a relief image. The resultant transparency will have a thickness variation approximately proportional to the phase of the wavefront (except for a constant term). The two transparencies sandwiched together forms the hologram.

The necessity of making a relief image can be avoided by the use of a reference beam to code the phase information as in an optical hologram[55]. To the (calculated) light wave coming from the object, $f(x,y)$, is added a reference beam, $r(x,y)$, and the result is squared to get

$$g(x,y) = |f(x,y) + r(x,y)|^2 \qquad \text{.....(6.1)}$$

If the reference beam is assumed to be a plane wave Ae^{icx} then

$$g(x,y) = |f(x,y)|^2 + A^2 + 2|f(x,y)| A \cos[cx - \phi(x,y)] \qquad \text{.....(6.2)}$$

where $\phi(x,y)$ is the phase part of the input wave $f(x,y)$. We then produce an intensity variation proportional to $g(x,y)$. A film is used to record $g(x,y)$ and by suitable processing the resulting transparency will have an amplitude transmittance proportional to $g(x,y)$ which is wholly positive.

To reconstruct the object the hologram is illuminated with a plane wave Ae^{icx}. The resulting light wave contains four components out of which one is proportional to $f(x,y)$, the original wave. By

suitably selecting a value for c in e^{icx}, the information carrying beam can be separated from the other three components.

Section 6.2 Binary Fourier transform holograms.

In this section we describe different methods of coding Fourier transform holograms. In the previous section, carrier wave (or reference wave) modulation was used as a convenient method to record complex wavefronts. In all the methods described below, without actually using a reference beam in our calculations, the same effect is achieved by what is known as 'phase coding' to represent complex signals. The holograms are binary diffracting elements and are designed to generate the required wavefront in one of the diffraction orders.

(A) Lohmann's method.

For a planar object, the light distribution at the Fourier plane, G, is first calculated.

i.e. $$G(u,v) = \int\int_{-\infty}^{+\infty} g(x,y) \exp -2\pi i (ux + vy)\, dxdy \quad \ldots\ldots\ldots (6.3)$$

where g(x,y) is the object function and u and v are the spatial frequency co-ordinates in the Fourier plane. (For Fourier-plane deblurring filters the filter function is calculated from the impulse response of the blur).

G(u,v) is then sampled in space. Suppose that we calculate G(u,v) at u,v = md; m = 0, 1, 2 -- and d = const. The sampled hologram is given by

$$G(u,v) = \sum_m \sum_n G(md, nd)\, \delta(u-md, u-nd) \quad \ldots\ldots\ldots\ldots (6.4)$$

where $\delta(u,v)$ is a 2-d delta function .

Each sample has, in general, a complex value and cannot be recorded on a film with density variations only . In Lohmann's hologram[56] each sample is represented by a completely transparent slit, the magnitude of the sample being proportional to the area of the slit. The phase at each point is represented as a shift in the position of the slit, proportional to the phase angle at that point. If the shifts in position (Δmn) are in the u direction then the Lohmann hologram can be represented mathematically as

$$G(u,v) = \sum_m \sum_n \left|G(md, nd)\right| \delta(u-md-\Delta_{mn}, v - nd) \quad \ldots\ldots\ldots\ldots (6.5)$$

where $|G(md,nd)|$ represents a fully transmitting area proportional to itself. Therefore Lohmann holograms are binary, each point in the hologram having a transmittance of either 0 or 1.

For reconstructing the object, the hologram is illuminated with a parallel beam of coherent light and G(u,v) is Fourier-transformed using a lens. The Lohmann hologram can be designed to reconstruct the original object in any one of the diffraction orders at the focal plane of a lens. It is common practice to have the object reconstructed in the first order, wherein the diffraction efficiency is a maxmimum.

A detailed mathematical analysis of the hologram, giving the approximations involved, due to digitization and restrictions to

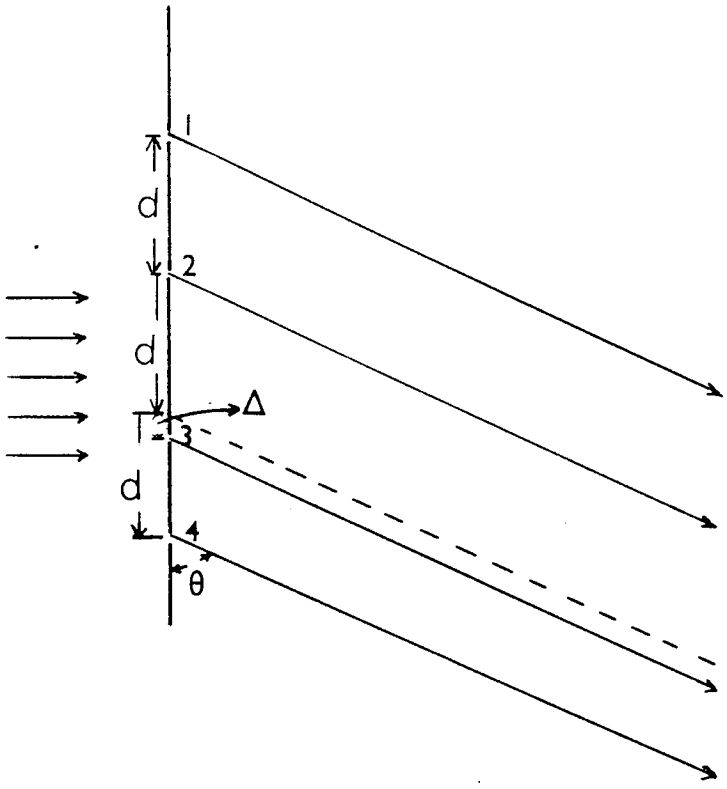

Fig.6.1. Side-view of a part of the Lohmann hologram. Samples 1, 2 and 4 occupy regular grid positions. Sample 3 is shifted by Δ.

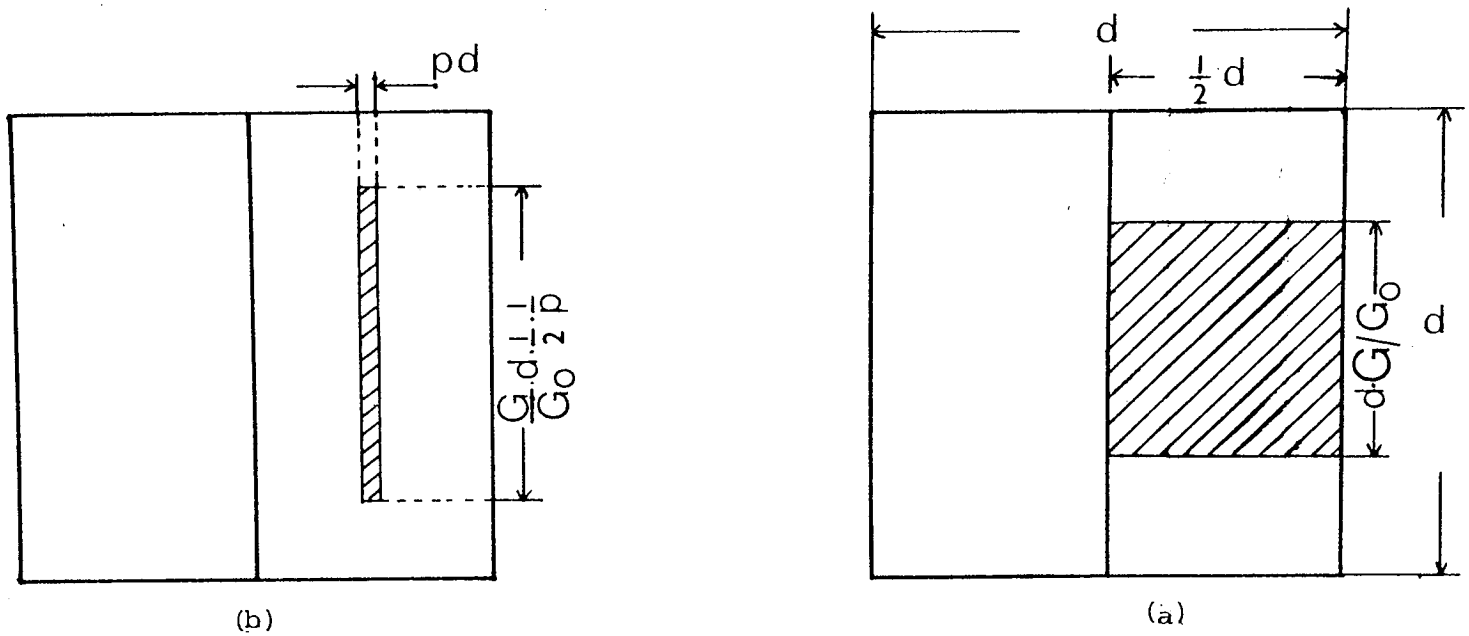

Fig.6.2. An individual cell in a Lohmann hologram filter. d x d is the size of one cell; G/G_o is the normalized amplitude being coded; pd is the pen-width; since the filter has only two phase values, the transmitting area is either located in the left or the right half of the cell. (a) if $G/G_o > p$ and (b) if $G/G_o < p$.

binary transmittance, is given by Lohmann and Paris[56]. Here we give a heuristic explanation of how the hologram works.

Figure 6.1 shows a side-view of a part of a Lohmann hologram. Samples 1, 2 and 4 have zero phase and they occupy regular grid positions. But sample 3 has a nonzero phase-angle (say ϕ_3) and hence is shifted from the normal grid position by a distance Δ proportional to ϕ_3. Light impinging from the left is diffracted and the far-field pattern is essentially the same as the Fourier transform of the hologram. Examining the far-field diffraction pattern at an angle $\theta = \text{Cos}^{-1}\ (\lambda/d)$ (λ is the wavelength of the light used) we find that the phase-differences between light from points 1,2 and 4 are multiples of 2π. We also notice that with respect to point 3 the phase differences for light from 1, 2 and 4 are 2π plus $\left(\frac{2\pi}{d}\right)\Delta$. So we see that the required phase relationship between the sample points is maintained if we choose Δ to make $\left(\frac{2\pi}{d}\right)\ \Delta = \phi_3$. Usually a lens is used to collect the diffracted light from the hologram and the far-field pattern coming in the θ - direction becomes the first order diffraction pattern.

A single cell from Lohmann's hologram is shown in Figure 6.2. The sampling cell size is d x d and the shaded area shows complete transmittance. With respect to the centre of the sample cell, the centre of the shaded area is shifter by Δ proportional to the phase of the wavefront at the sampling point. If G_o is the maximum value of the amplitude (G) to be plotted and if p^d is the penwidth of the plotter used, then Figure 6.2 a & b show the openings for $G/G_o > p$ and $G/G_o < p$ respectively. The maximum diffraction efficiency of a

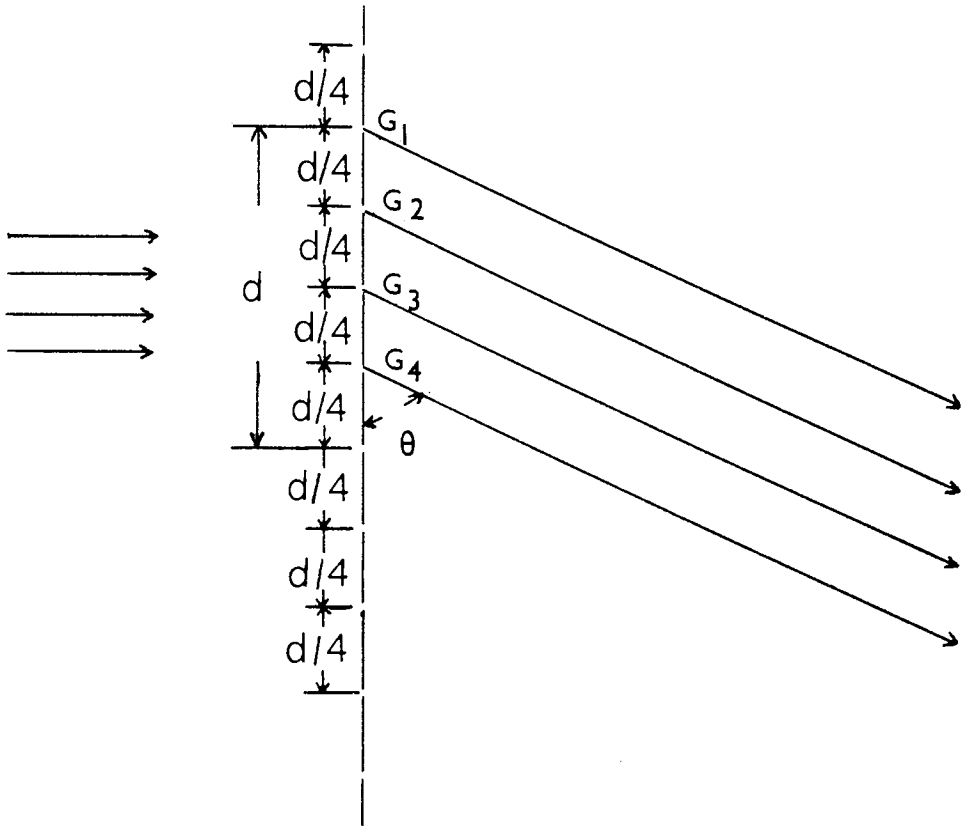

Fig.6.3. Side-view of a part of the Lee hologram. Each complex sample is represented by four equally spaced openings G_1, G_2, G_3 and G_4.

binary hologram is 10%. Like other binary holograms Lohmann hologram is free of stringent photographic processing.

(B) Lee's hologram and Burckhardt's modification

Another technique which utilizes detour phase variation in the diffraction image is due to Lee[63]. Here, each complex valued sample G(md,nd) is split up into four positive real components in the hologram. Let G_r and G_i be the real and imaginary parts of G respectively. Also assume that

$$G_1 = \begin{cases} G_r & \text{if } G_r \geq 0 \\ 0 & \text{if } G_r < 0 \end{cases} \quad \ldots\ldots\ldots\ldots (6.6)$$

$$G_3 = \begin{cases} -G_r & \text{if } G_r < 0 \\ 0 & \text{if } G_r \geq 0 \end{cases} \quad \ldots\ldots\ldots\ldots (6.7)$$

$$G_2 = \begin{cases} G_i & \text{if } G_i \geq 0 \\ 0 & \text{if } G_i < 0 \end{cases} \quad \ldots\ldots\ldots\ldots (6.8)$$

$$G_4 = \begin{cases} -G_i & \text{if } G_i < 0 \\ 0 & \text{if } G_i \geq 0 \end{cases} \quad \ldots\ldots\ldots\ldots (6.9)$$

Then we can write $G = G_1 - G_3 + iG_2 - iG_4$ ..... (6.10)

where all the components G_1, G_2, G_3 and G_4 are real and positive.

Fig.6.3 is a side-view of a part of a Lee hologram. Each complex valued sample is described by four equally spaced slits representing the components G_1, G_2, G_3 and G_4. For optical reconstruction, as with Lohmann hologram the hologram is illuminated with a parallel beam of light. The far-field diffraction pattern is observed at an angle $\theta = \text{Cos}^{-1}(\lambda/d)$. We notice that the path

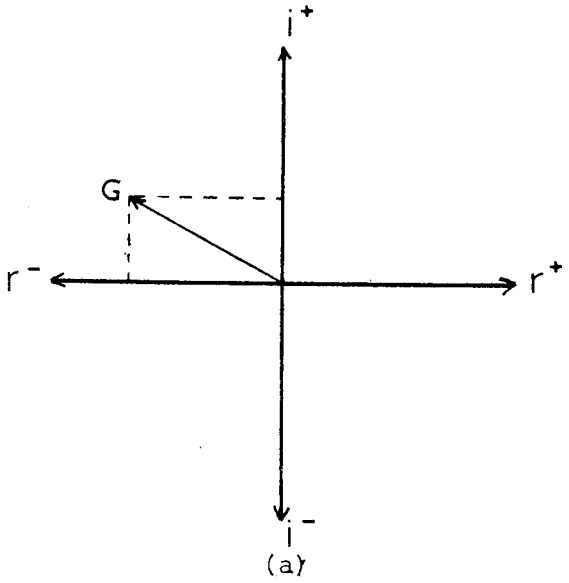

(a)

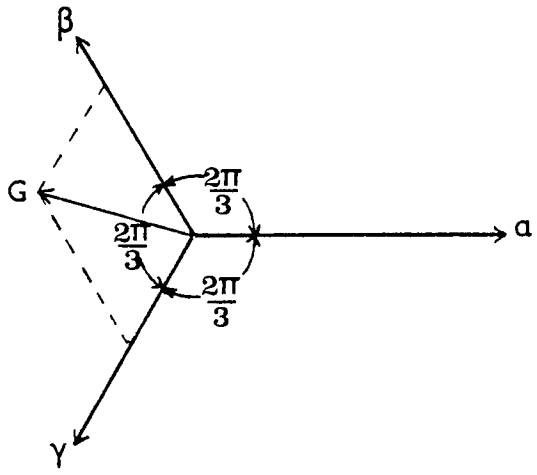

(b)

Fig.6.4. (a) Resolving the complex sample into four positive real components (Lee's method).
(b) Burkhardt's simplification to reduce the number of components to three.

differences of light from G_2, G_3 and G_4 with respect to G_1 are respectively $\lambda/4$, $\lambda/2$ and $3\lambda/4$. The corresponding phase differences are $\pi/2$, π and $3\pi/2$ respectively and $\exp(i\pi/2) = i$, $\exp(i\pi) = -1$ and $\exp(i3\pi/2) = -i$. So, in the first diffraction order, this is tantamount to multiplying G_1, G_2. G_3 and G_4 by 1, i, -1 and -i respectively and taken together they give the complete sample G of Eq.(6.10).

Optical density variations can be used to represent the four positive components of each of the complex samples. In this case, generation of a Lee hologram requires grey-level plotting. Alternatively, the amplitude can be represented as transmitting area variations (as in the case of a Lohmann hologram) which gives a binary Lee hologram. Like the Lohmann hologram the diffraction efficiency of the binary Lee hologram has a maximum value of 10%.

Equation (6.10) can be interpreted as a vector resolution in the complex-number plane, as shown in Figure 6.4a. Here, vector G is represented using a set of four base vectors.

$$r^+ = (1,0),\ r^- = (-1,0),\ i^+ = (0,1) \text{ and } i^- = (0,-1).$$

For any vector we can write

$$G = G\, r^+ + G_2\, i^+ + G_3 r^- + G_4 i^- \quad \ldots\ldots\ldots\ldots\ldots\ldots \quad (6.11)$$

where G_1, G_2, G_3, and G_4 are all positive. From this we see that at most two of the four components can be non-zero. This fact has led Burckhardt[64] to make the interesting suggestion which reduces the number of base vectors required to represent a complex vector from four to three. The base vector, α, β and γ (Figure 6.4b) employed

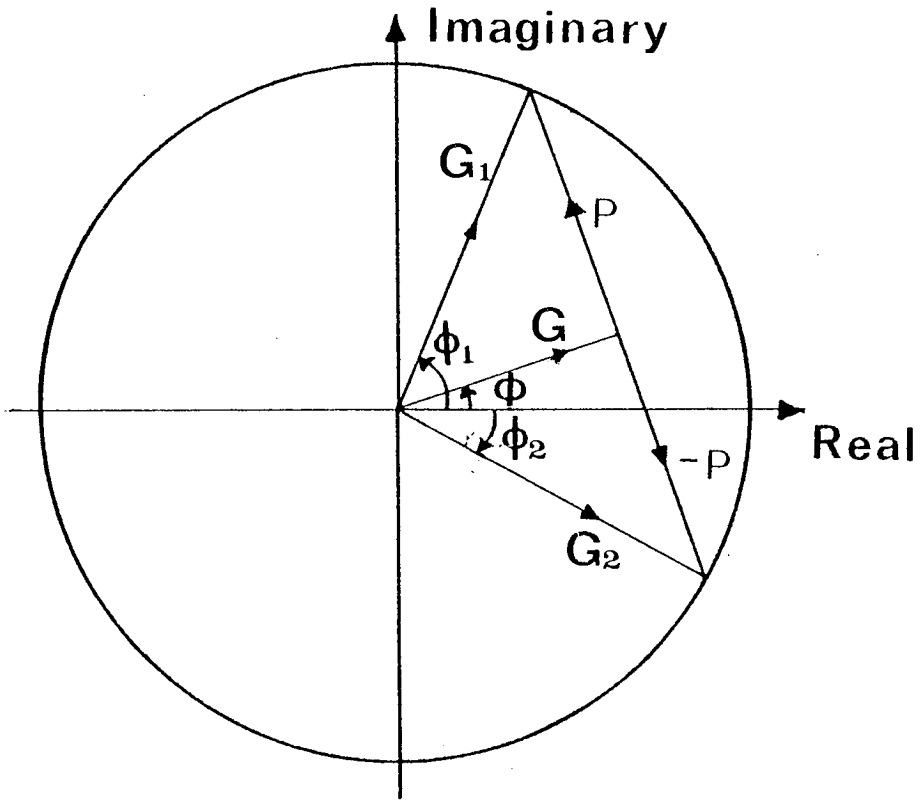

Fig. 6.5. Splitting a complex number G (representing the filter function) into two constant magnitude vectors, G_1 and G_2, by the parity pair P and -P.

by Burckhardt are sufficient to represent any complex vector G as

$$G = a\alpha + b\beta + c\gamma \quad \ldots\ldots\ldots\ldots\ldots\ldots\ldots\ldots (6.12)$$

where a, b and c are all positive. The base vectors subtend an angle $2\pi/3$ with each other and it is seen that at most two of the components are nonzero.

Burkhardt's suggestion reduced the number of subcells in the hologram from four to three. Davies[65] suggests a method of coding complex values after introducing what is known as a parity vector pair into each of the complex samples thereby splitting the sample into two complex vectors of unit magnitude. Hsueh and Sawchuk[60] developed the idea further to generate what they call double phase holograms (DDH) of 2 - d objects. In the next sub-section we give a brief mathematical description of the DPH without going into any rigorous details. (A detailed analysis of the DPH with special emphasis on noise due to phase coding errors and cell displacement can be found in reference 60).

(C) The Double Phase Hologram (DPH)

The DPH is a result of direct development from the spectrum levelling technique first described by Chu and Goodman[61]. Spectrum levelling technique can be easily understood with reference to the diagram shown in Figure 6.5, which is an Argand diagram showing a complex vector G. G in our case is a complex transmittance function representing, say, a wavefront or a Fourier transform, or the transfer function of a blur. The circle in Figure 6.5. is taken to be a unit circle with the radius representing the maximum value of the

function we are coding. To each complex vector G is added and subtracted another vector P in such a way that the resultant vectors

$$\left.\begin{aligned} G_1 &= G + P \\ G_2 &= G - P \end{aligned}\right\} \qquad \text{.....(6.13)}$$

have a constant (here, unit) magnitude

In other words, a complex transmittance function can be split up into two constant magnitude vectors,or

$$|G|\, e^{i\phi} = e^{i(\phi + \phi_1)} + e^{i(\phi - \phi_1)} \qquad \text{.....(6.14a)}$$

where $\varphi_1 = \text{Cos}^{-1}\ (|G|/2)$ ..... (6.14b)

Since $|G|$ lies between 0 and 1 in the case of a filter transmittance function, ϕ_1 takes value only between $\pi/3$ and $\pi/2$. From this we see that ϕ_1 is restricted to a narrow range of values. This range can be enhanced by assuming that the modulus of the constant magnitude vectors is 1/2 instead of unity. (We must bear in mind that $|G|$ has a range from 0 to 1).

So we alter Equation (6.14) to

$$|G|\, e^{i\phi} = \frac{1}{2}\left\{ e^{i(\phi+\phi_i)} + e^{i(\phi - \phi_1)} \right\} \qquad \text{.....(6.15b)}$$

where $\phi_i = \text{Cos}^{-1}(|G|\ )$ .....(6.15b)

Here ϕ_1 has a range from 0 to $\pi/2$.

These two constant magnitude vectors can be represented,

following Lohmann's coding, by two constant area slits separated by a distance proportional to ϕ_1. As opposed to Lohmann hologram one advantage of the DPH is its ability to code very small amplitude values, while a Lohmann hologram is limited by the finite plotter pen resolution. However, the DPH is limited by the coarse phase quantization levels in the hologram which introduces noise in the reconstruction, at the same time adversely affecting the resolution

We have considered here various ways of generating binary Fourier transform holograms. In this chapter our aim is to explore the possible application of binary hologram, as deblurring filters. However, before we go into the application of binary holograms in spatial filtering and the description of the experiments done, we would like to discuss two important constraints on computer generated binary holograms, namely sampling rate limitation and errors introduced due to quantization .

Section 6.3. Sampling Rate Limitation and Quantization errors.

In computer generation of holograms, the hologram space is sampled and the amplitude and phase values of the samples are quantized to a finite number of levels. Both sampling and quantization affect the final performance of the hologram.

(A) Sampling-rate limitation

When the Fourier transform $G(u,v)$ of an object is recorded as a binary hologram using one of the methods described earlier, it can be

shown that the reconstruction (i.e. the inverse Fourier transform of the hologram) consists of a sum of periodically shifted terms. Assuming that the object (or impulse response) is band-limited and having a finite extent, it can be expanded using a Fourier series containing a finite number of terms. Strictly, the Fourier series represents a repeated object distribution of certain finite periodicity and hence any reconstruction from this discrete spectrum is expected to exhibit the same periodicity. Or, in other words, sampling (or discrete nature) in frequency domain produces replication in space domain and vice versa.

When the Fourier transform of an object g(x,y) of limited extent (say, L x L) is sampled, the reconstruction from the sampled spectrum results in a replicated output. Let the sampling period for the object spectrum G(u,v) be Δu and Δv. Then, using Whittaker-Shannon sampling theorem[66], the optical reconstruction from the sampled hologram will be

$$\tilde{g}(x,y) = \sum_m \sum_n g\left(x - \frac{m}{\Delta u}, y - \frac{n}{\Delta v}\right) \qquad \ldots\ldots\ldots\ldots (6.16)$$

We require that these periodically shifted versions of the object function to be non-overlapping. For that we should have

$$\left.\begin{aligned} \Delta u &\leq \frac{1}{L} \\ \Delta v &\leq \frac{1}{L} \end{aligned}\right\} \qquad \ldots\ldots\ldots\ldots (6.17)$$

Since the object is assumed to be band-limited the Fourier transform hologram is of finite extent, say W x W. To avoid overlapping of various reconstructions we sample the hologram at a period $\Delta u = \frac{1}{L}$ and $\Delta v = \frac{1}{L}$. The total number of samples required

for the entire hologram is then $(WL)^2$.

When Lohmann's or Lee's method of coding is used to represent a Fourier transform hologram, the reconstruction again consists of a sum of periodically shifted terms. However, these terms are not just shifted replicas of each other. Lohmann's or Lee's hologram reconstructs the original object faithfully only in one of the diffraction orders, along the direction of phase-coding. Since the first diffraction order has the maximum light availability, we usually design the hologram to reconstruct the object in the first order. The other terms in the reconstruction are generally related to the original object in a complicated manner, Experimental evidence indicates that each of these terms has the same size as the original object and hence to avoid overlapping in the reconstruction, Equation (6.17) can be used as a guide-line.

In binary Lohmann hologram the magnitude of a complex sample is represented as a transmitting area in an opaque background with the centre of the area shifted (in the u-direction, say) by an amount proportional to the phase of the sample, from the centre of the cell. Therefore, if we are using WL samples over the width of the hologram then the resolution requirement in the u-direction will be WLsm; and the resolution requirement in the v-direction will be just WLn. Here, s, is the number of phase quantization levels we use and m x n the number of quantization levels for the amplitude of the Fourier transform. In the case of Lohmann filters for correcting linear motion blur and defocusing, since the blur transfer functions take only two phase values, namely 0° and 180°, s is equal to 2.

Since we are coding the phase angles in u direction, it is common practice to code the amplitude values of the Fourier transform entirely in the v-direction. In other words, if we use rectangular openings to represent samples of the blur function, then the width of the openings (along u direction) remains the same throughout the filter while the height of the opening is quantized to m x n levels to represent the amplitude variation.

In a Lee hologram we represent a complex sample by four positive real samples (phase coded in u direction, say) and hence the resolution requirement in u and v directions are 4WL.m and WL.n cells respectively choosing to have m and n amplitude quantization levels along u and v directions respectively.

In a double phase hologram, the amplitude is represented as a phase variation(coded, say, along u direction). Then, assuming that there are only two phase angles in the filter function we are coding then the resolution requirement in u direction is m x n.WL.2. Along v direction the resolution requirement is WL. As before, m x n is the number of quantization levels of the amplitude (here, represented as a phase angle variation). We notice that the overall resolution requirement of the DPH remains the same as that of an ordinary Lohmann hologram.

When using for image deblurring the binary hologram filter should have a space bandwidth product at least as large as that of the object, in order that the information bearing first order is well separated from its adjacent neighbours. This means that for processing large objects the filter needs a very large plotting time. Chavel and Lowenthal[47] have suggested a method of circumventing this difficulty

for those blurs whose impulse response is small compared to the object. Chavel and Lowenthal's method is essentially plotting a filter of small space-bandwidth product and using the image formed by the information bearing first order spectrum from this filter to form a 'natural hologram' with a reference beam. By adjusting the reference beam angle the space-bandwidth product of the natural hologram can be enhanced to be higher than that of the object to be deblurred. Such a 'natural hologram' forms the high space-bandwidth product deblurring filter.

(B) Quantization

When the number of quantization levels used is large, Anderson and Huang[67] modelled the quantization noise as white noise independent of the signal being quantized and analysed the effect of quantization in various types of Fourier transform holograms. In a Lohmann hologram the noise is added to the magnitude and phase of the Fourier transform, while in the Lee hologram the noise is added to the real and imaginary parts.

Uniform quantization of the magnitude or the real and imaginary parts of the Fourier transform introduces white noise in the amplitude of the reconstructed image. When recording the intensity of the image, this noise becomes multiplicative. The effect of uniform phase quantization is to introduce additive noise in the amplitude of the reconstructed image whose power spectral density is proportional to the square of the Fourier spectrum of the original image. This noise contains largely low frequencies. (As

is characteristic of most of the images). While considering intensity the noise again becomes multiplicative.

When the number of quantization levels is small a more exact analysis becomes necessary. Such an analysis in the case of phase quantization can be found in Goodman and Silvestri's[68] work. For 1-d case the result can be summarized as follows :

In the Fourier transform $G(u) = |C(u)| \exp\{i\phi(u)\}$ of $g(x)$ we quantize $\phi(x)$ alone; then the inverse Fourier transform becomes

$$g'(x) = \sum_{m=-\infty}^{-\infty} \operatorname{sinc}(m + \frac{1}{N})\, g_m'(x) \quad \ldots\ldots\ldots\ldots\ldots \quad (6.18)$$

where $$g_m'(x) = \int_{-\infty}^{+\infty} |G(u)| \exp(i)\{Nm + 1)\ \phi(u) \exp(i2\pi u)\, du \quad \ldots\ldots\ldots\ldots\ldots (6.19)$$

and N is the number of quantization levels used for $\phi(u)$.

Note that $g_o'(x) = g(x)$.

If we suppose that $g(x)$ is a small object in a large opaque field, then $g_m'(x)$ for $m \neq 0$ are shifted versions of $g_o'(x)$. If $g(x)$ is diffuse then $g_m'(x)$ is approximately the $(Nm + 1)^{th}$ order self convolution of $g_o'(x)$.

Section 6.4. Generation of deblurring filters :-

(A) As Lohmann's holograms : -

The blur transfer function for linear motion blur (a sinc function) and defocusing ($J_1(cr)/cr$) are calculated from the *a priori* knowledge of the amount of blur. This information is used to calculate the corresponding Wiener filters. (The noise parameter, ε, is fixed at 0.05). The Wiener filter is then sampled uniformly as a 80 x 80 matrix.

The samples are represented using Lohmann's method. The following procedure is adopted to generate the hologram.

The plotting area is divided into 80 x 80 square cells of equal area. Each cell representing one of the 80 x 80 samples of the Wiener filter function is divided into two halves. (Say, along the u direction in which the phase is coded.) Either the left or the right half is selected, depending on whether the phase of the filter function at that point is 0° or 180°. (Selection of the right or left half to represent either 0° or 180° phase is arbitrarily done at the start and once the selection is made the same is maintained throughout the filter) . Centred on the half selected is drawn a rectangle with base equal to half the width of the sampling cell (d) and height equal to the normalized amplitude (G/G_o) at that point multiplied by the length of the sampling cell. (Figure 6.2a). The rectangle is shaded either by ink (if using a pen plotter)or by filling in with light (if using a picture processing peripheral like FR80). This procedure is adopted so long as we have $\left(\frac{G}{G_o}\right) d \geq pd$ where pd is the penwidth of the plotter (or the minimum resolvable distance in the cathode ray tube of the FR80). When $\left(\frac{G}{G_o}\right) d < pd$ we slightly modify the procedure as follows. Instead of drawing a rectangle we draw a line, perpendicular to the direction of phase-coding, of length equal to $\left(\frac{G}{G_o}\right) d \cdot \frac{1}{2} \cdot \frac{1}{p}$ (Figure 6.2b). Thus the total area shaded in both the cases is proportional to the amplitude of the filter sample at that point, the constant of proportionality remaining the same.

We have used an image processing peripheral (FR80) attached to an IBM 360 computer to do the plotting. The FR80 has a plotting area which has 16384 separately addressable points (raster units) in both x and y

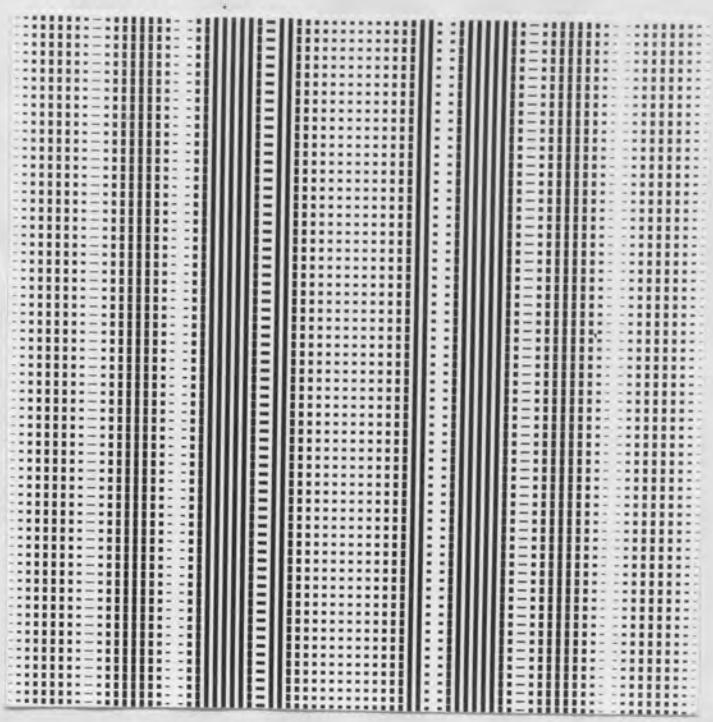

(a)

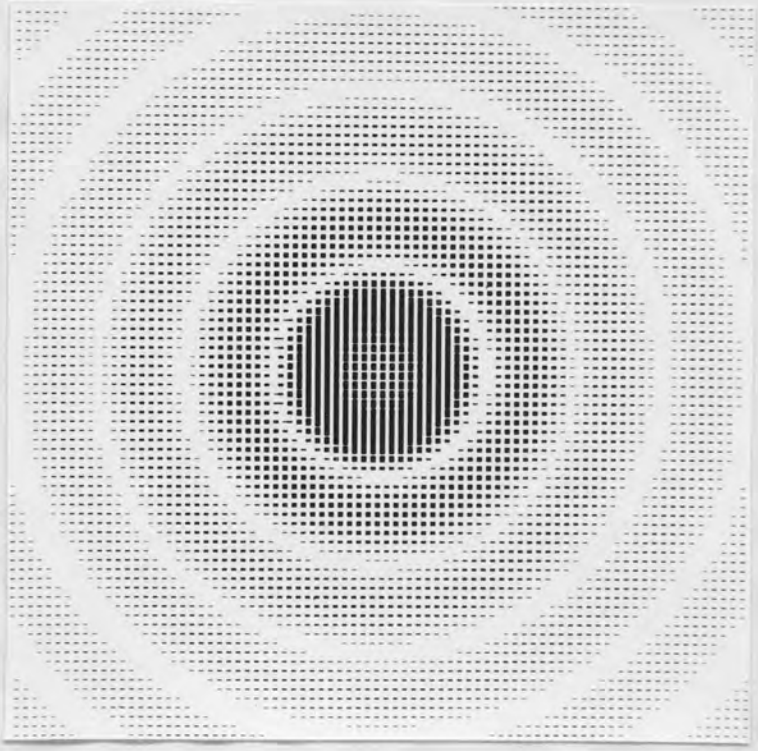

(b)

Fig.6.6. Enlarged photograph of the Lohmann Wiener filter (ε = 0.05);
(a) for linear motion blur
(b) for defocusing.

directions. Each raster unit is, while using a 35mm camera, equivalent to 0.0000596". There are built in programs to fill in (with light) the required areas.

Using FR80 we have produced two Wiener filters (proportional to $H^*/(|H|^2 + \varepsilon)$ the first with $H = \frac{\text{Sin } u}{u}$, the second with $H = \frac{J_1(cr)}{cr}$). ε is kept in both the cases at 0.05. The filters are shown in Figure 6.6. Highly magnified versions of the filters produced on hard copy paper are photo-reduced onto high resolution plates (Agfa 10E56) using a camera fixed on vibration free mounts. The final size of the filter is determined by the amount of blur the input picture has undergone and the focal length of the transforming lenses and the wavelength of laser used in the optical processing system. (The optical processing system is described in Chapter 3).

(B) As DPHs

We now describe how we developed deblurring filters as DPHs. In the case of linear motion blur which is an 1-d blur, the Wiener filter has no transmittance variation perpendicular to the direction of the blur. In this case, the filter can be generated as a grating with lines running perpendicular to the direction of the blur. Each period of the grating contains two lines forming a doublet. Each of the lines in the doublet represents one of the two constant magnitude vectors into which the filter transmittance function at that point is divided. The separation between the lines is proportional to ϕ_1 (Eq.6.15b) and is therefore related to the modulus of the filter transmittance function. The width of the lines (throughout the filter) remains constant and is not related to the amplitude value of the filter. (However, the linewidth considerably affects the diffraction efficiency

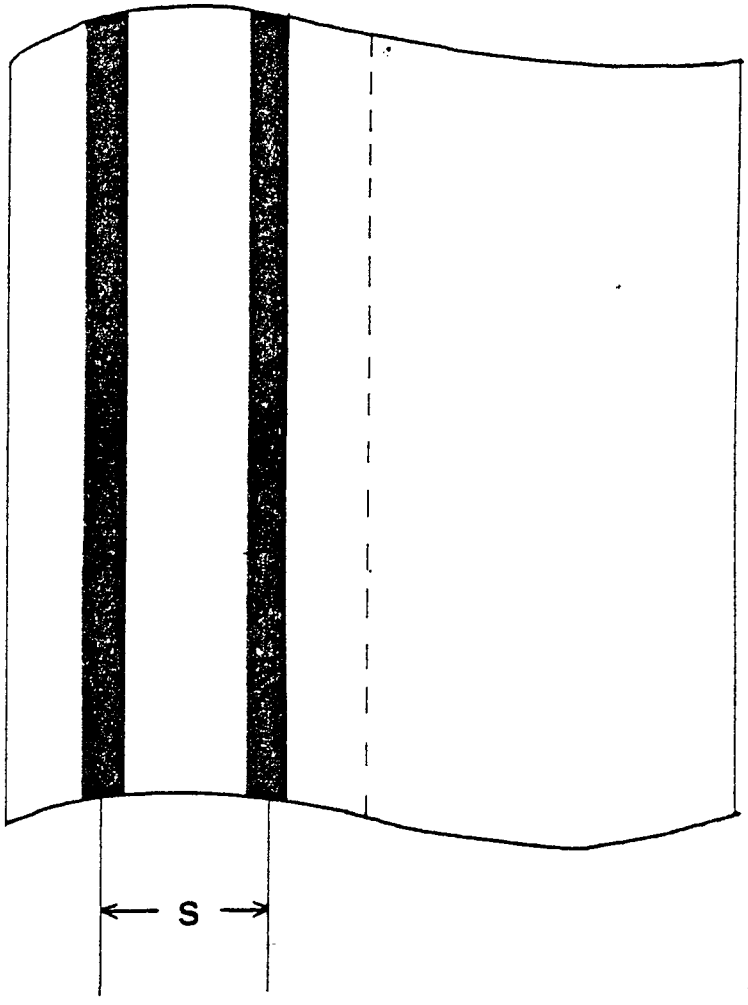

Fig.6.7. A part of the double-phase hologram filter for linear motion blur showing one period. The doublet separation s is proportional to ϕ_1 of Eq.6.15b. (See text).

of the filter; and we are concerned about diffraction efficiency since we get the deblurred output in the first order diffraction spectrum of the DPH. Nevertheless we cannot choose a linewidth that gives the maximum diffraction efficiency in the first order, because, by doing so we will be sacrificing the space available in the cells (or periods) to code the variation of ϕ_1 (Eq.6.15b). We choose to sacrifice diffraction efficiency (small diffraction efficiency only means a larger deblurring exposure time) for a smoother representation of the amplitude variation, that results in a better resolved output). Each period of the DPH is divided into two halves and the doublet is drawn on either the left or the right half of the period only, depending on whether the filter transmittance at that point is positive or negative. Fig.6.7 shows a part of one of the periods of the DPH filter for linear motion blur. Here, the left half is chosen for drawing the doublet. The separation between the lines in the doublet is proportional to ϕ_1.

The blur transfer function for defocusing has no line symmetry. (In fact, it is circular symmetric .) Consequently, while plotting, the doublets in individual cells, have to be plotted one after another. The plotting of this filter obviously takes longer than that for linear motion blur.

A deblurring filter has, in general, a large transmittance range and from Eq.6.15 we see that the phase introduced by the parity terms has only a range from 0 to $\pi/2$. This means that the amplitude values undergo big jumps when moving from one sample cell to another and hence we have a coarse amplitude quantization in the filter. This problem can be overcome to an extent by splitting the amplitude part

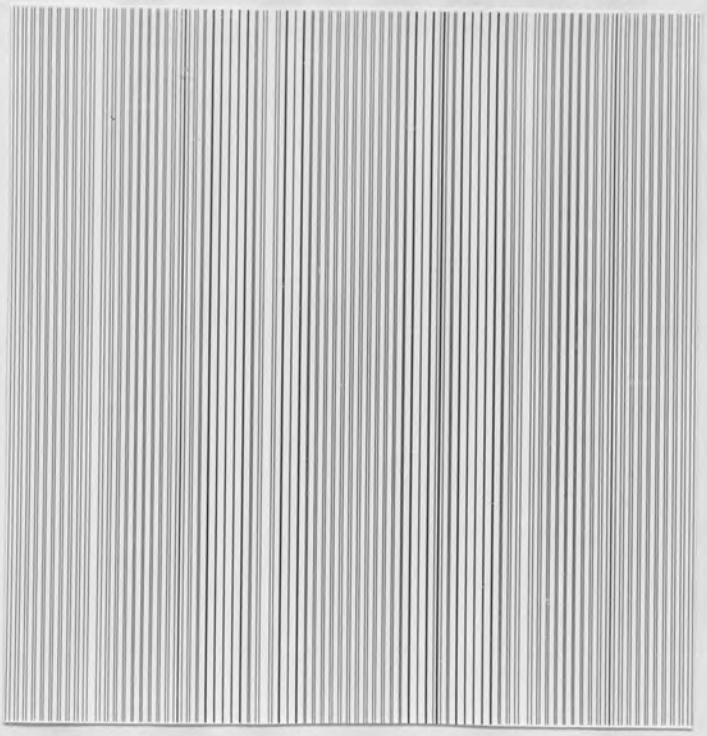

(a)

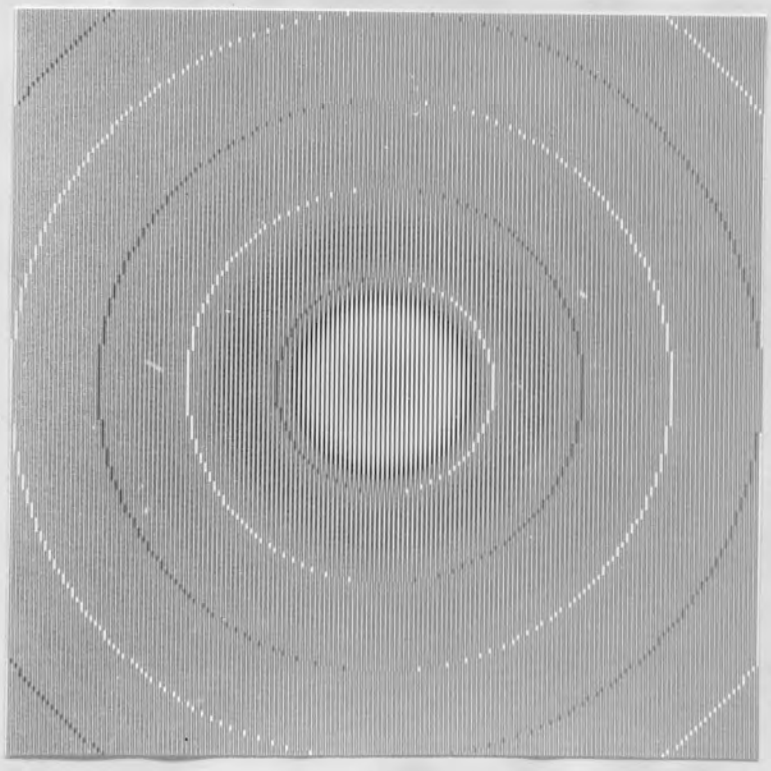

(b)

Fig.6.8. Photographs of the double-phase hologram deblurring filter containing full amplitude part (G); (ε = 0.075)

(a) linear motion blur

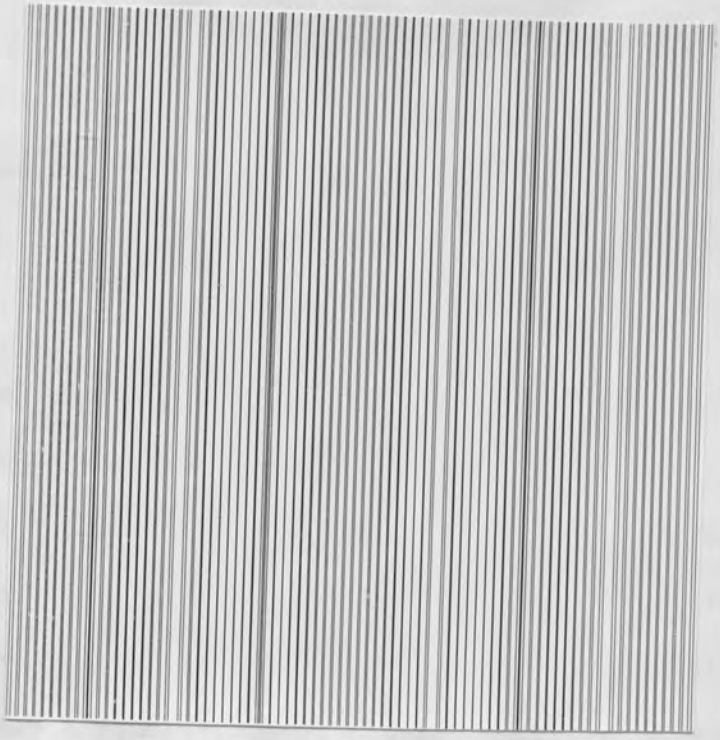

(a)

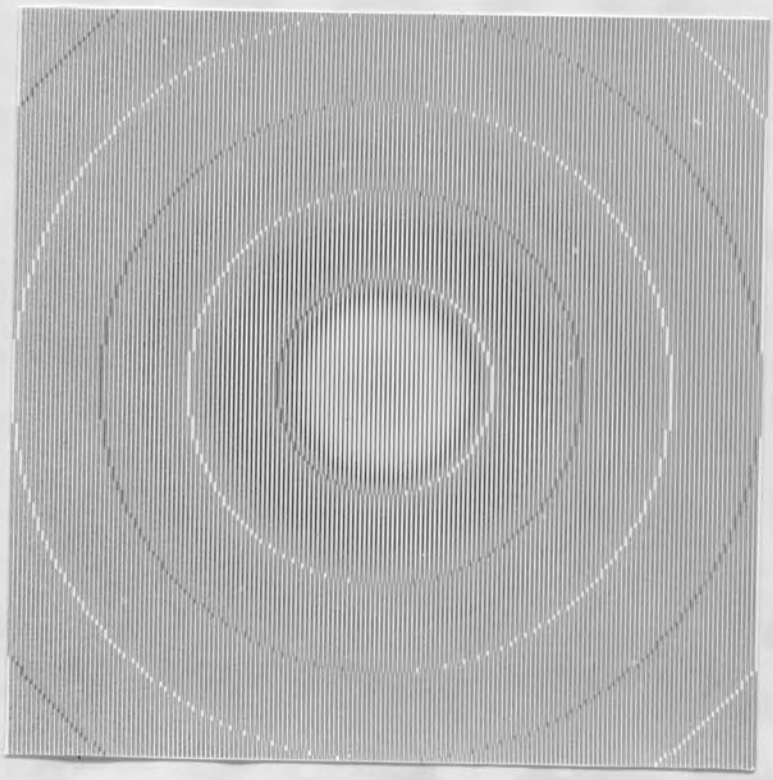

(b)

Fig. 6.9 Photographs of the double-phase hologram deblurring filter containing only $G^{\frac{1}{2}}$; ($\varepsilon = 0.075$)
(a) linear motion blur
(b) defocusing

of the filter ($|G|$) into two $G^{1/2}$s. The first $G^{1/2}$ is incorporated into the DPH and the second $G^{1/2}$ is made as a density variation on a photographic film. The two parts are sandwiched together to give the required filter function.

Here, we have generated with the help of the FR80 four DPHs. The first and second are Wiener filters for linear motion blur and defocusing respectively. (The noise parameter, ε, in all the cases was kept at 0.075) They are shown in Fig.6.8. The third and fourth DPHs are again Wiener filters for motion blur and defocusing this time incorporating only a square-root of the respective Wiener filter amplitude transmittance. They are shown in Fig.6.9.

Section 6.5

Experimental

Both the motion blurred and out-of-focus objects were prepared in the laboratory using a simulation method described by Goodman[42]. (The details of the photographic process used to get the right gamma value are given in Chapter 3).

The optical processing system used is the same as the one described in Chapter 3 (Fig.3.9). The laser L, beam expander BE and the collimator C combine to give a parallel beam of light illuminating the blurred object, mounted in plane O which is one of the focal planes of the lens L_1. (The object is immersed in cedarwood oil gate to compensate for any phase distortions introduced by the film non-uniformities). The Fourier spectrum of the object is formed by the

(a) (b)

(c)

Fig.6.10. The blurred objects.
(a) Linear motion blur.
(b) Defocusing.
(c) Linear motion blur.(large object).

lens L_1 at its second focal plane F. The corrected spectrum is recombined by the lens L_2 to form the deblurred output at O. Since the filters here are binary holograms designed to give the correct output in the first order spectrum, the deblurred pictures are observed in the first order images from the filter.

First, the linear-motion blurred picture shown in Fig. 6.10a is deblurred using both the Lohmann hologram filter and the DPH Wiener filter. (incorporating full amplitude transmittance). The deblurred outputs (Fig.6.11a & b) show a great deal of enhancement. The resolution seems to be affected due to the coarse quantization levels in the filter and also due to the high frequency attenuation caused by the Wiener filter.

Second, the out-of-focus picture of Fig. 6.10b is similarly deblurred using both the Lohmann filter and the DPH filter. From the outputs shown in Figs.6.12a & b we notice that the degree of deblurring achieved for out-of-focus pictures is not as high as that for pictures affected by motion blur. (The same observation is made in Chapter 4, from a comparison of results from Chapter 3. The reasons given in Chapter 4 for this drop in performance are applicable here as well).

Third, sandwich filters combining the DPH filters and the photographically generated filter, each containing $G^{1/2}$ of the Wiener filter amplitude transmittance $|G|$, were used to deblur both the linear motion blurred and out-of-focus objects. (The photographic part of the filter for the 1 - d blur is generated using the cylindrical

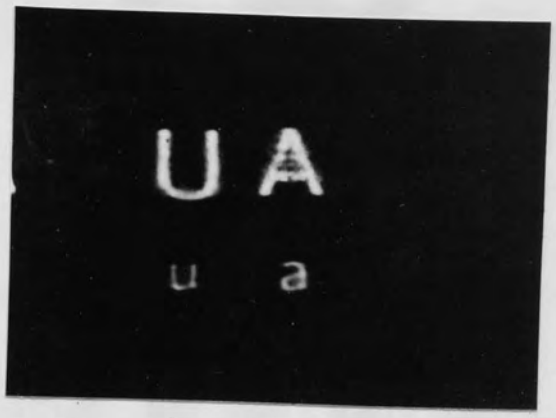

(a)

(b)

(c)

Fig.6.11. The deblurred outputs from the linear motion blurred object (Fig.6.10(a)).
(a) using Lohmann hologram filter.
(b) using the double phase hologram filter.
(c) using a sandwich filter containing the double-phase hologram filter, and the photographically generated amplitude mask.

(a)

(b)

(c)

Fig.6.12. The deblurred outputs from the out-of-focus object (Fig.6.10(b)).
(a) using Lohmann hologram filter.
(b) using the double phase hologram filter.
(c) using a sandwich filter containing the double-phase hologram filter, and the photographically generated amplitude mask.

lens method as given in Chapter 3. The rotating disc method of Chapter 4 was used in the case of 2-d blur). The deblurred outputs (Figs.6.11c and 6.12c) show an improvement in resolution.

The first order spectrum of the DPH filter for $G^{1/2}$ is allowed to form an image, while the other orders are blocked. The image recorded and shown in Fig.6.13a gives an idea of the amplitude variation encoded in the filter. This can be compared with the photographically generated part of the filter which is shown in Fig.6.13b.

Finally, we describe how we have generated a large space-bandwidth product 'natural hologram' from a low space-bandwidth product DPH filter. The set-up shown in Fig.6.14 is the same as the optical processing system shown in Fig.3.9 of Chapter 3, but for a beam-splliter and mirror arrangement for providing a reference beam in the output plane O. The input plane I has the low space-bandwidth product DPH filter (Here we have used the one for linear motion blur). The filter plane F has an opaque screen with a narrow opening to let in only the first order spectrum from the DPH. The image formed by this first order spectrum is combined with a reference beam R coming at an angle θ to the optical axis of the system. The spatial frequency content of the hologram formed at plane O depends on θ and hence the space-bandwidth product of the final hologram can be enhanced as required by fixing θ appropriately. The natural hologram was used to deblur the large object shown in Fig.6.10c. The lens L_2 of Fig. 3.9 had to be moved sideways to admit the first order diffracted image from the natural hologram. The deblurred output is shown in Fig.6.15.

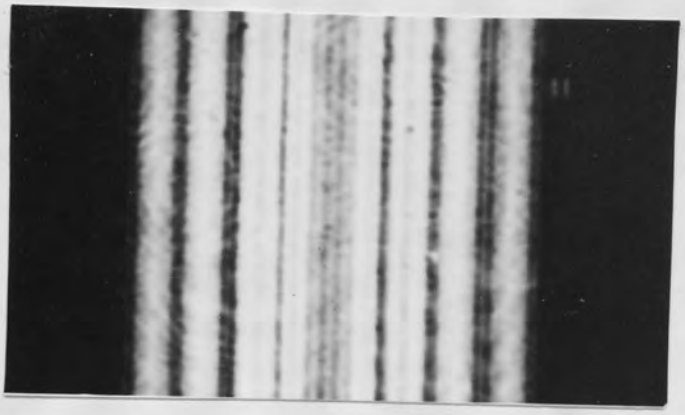

Fig.6.13(a) The image formed by the first order spectrum of the double phase hologram filter for linear motion blur. The intensity variation across the image indicates the amplitude encoding in the filter.

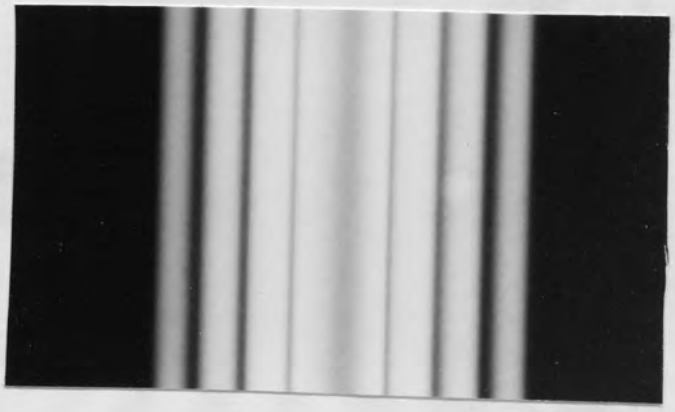

Fig.6.13(b). The amplitude filter obtained by the cylindrical lens method. This compares well with the intensity variation shown in Fig.6.13 (a).

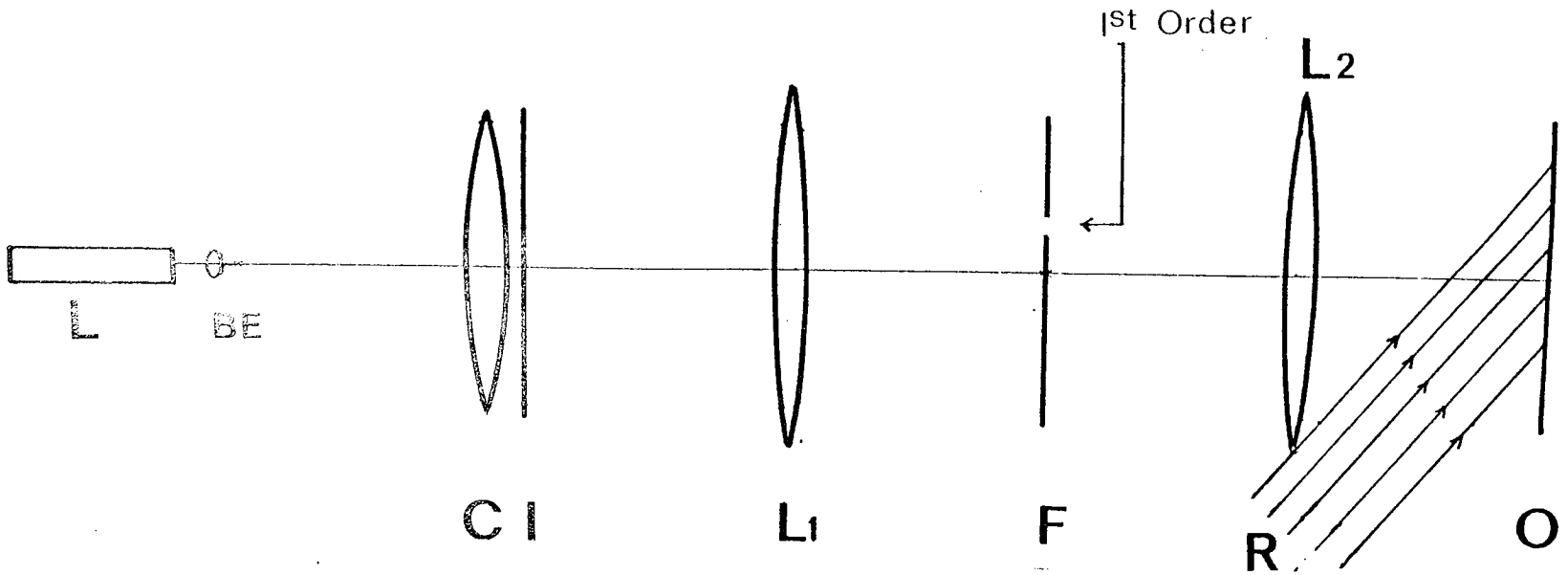

Fig.6.14. The set-up for generating the actual hologram. The double-phase hologram in plane I is Fourier transformed by lens L_1. The first order spectrum let through by the mask in plane F is retransformed by lens L_2. The reference beam R is derived from the same source L by a beam splitter.

FIG.6.15 The deblurred output from the 'natural hologram filter'

Section 6.6

Conclusion

We have briefly considered different methods of forming binary holograms. Deblurring filters for correcting out-of-focus pictures and linear motion blurred pictures were generated as both Lohmann holograms and double phase holograms. The deblurred outputs show a good deal of enhancement especially in the case of motion blurred pictures. We found that, in general, the 2-d circular blur was more difficult to deconvolve than the 1 - d linear motion blur and the quality of the outputs obtained for the former case was somewhat inferior. The output resolution seems to be affected by the coarse amplitude quantization in the filter function. We have reduced the problem of poor resolution by replacing the binary hologram filter by a combination of a photographically produced filter and another binary hologram, each representing a square-root of the required Wiener filter amplitude transmittance. The experimental result of deblurring shows an improvement in output resolution in the case of a DPH filter backed by a photographically produced amplitude component. We have increased the space-bandwidth product of a binary hologram filter by forming a 'natural hologram' from its first order spectrum.

The enhanced pictures obtained lead us to believe that binary holograms open up an easy way of fabricating good performance Wiener deblurring filters.

C H A P T E R 7

CONCLUSIONS

We have discussed in this work different methods of developing deblurring filters for use with a coherent optical processing system. All the filters generated here work in the Fourier plane, appropriately modifying the Fourier spectrum of the blurred object.

Of the two blurs tackled, linear motion blur and defocusing, the first one gave better results throughout. Total lack of redundancy and errors in the amplitude filter due to film nonlinearities are the main reasons for the inferior deblurred outputs in the case of defocusing. The phase filters developed by photomechanical means gave satisfactory phase inversions.

Straightforward inverse filtering of linear motion blurred objects in Chapter 3, resulted in the enhancement of high frequency noise as well and the result obtained was marred by noise. Use of a Wiener filter with $\varepsilon = 0.1$ suppressed all the noise, but caused high frequency attenuation resulting in loss of resolution in the output. With $\varepsilon = 0.05$ we got a satisfactory noiseless output with the resolution not seriously affected.

The use of phase filter is altogether eliminated by subjecting the blurred object to a further blur of the same amount. Since the resultant blur transfer function is the square of the transfer function for the original blur, the transmittance range of the correcting filter to be generated is very high. Consequently, we are again faced with the problem nonlinearities introduced by the recording emulsion. We

met this problem by building up the filter as a sandwich of 3 components, each having a transmittance proportional to the cube root of the transfer function for the combined blur. The output, though suffering from loss of information at certain places, shows a certain amount of improvement.

Binary hologram deblurring filters developed in Chapter 6 gave good results, especially in the case of linear motion blur. Because the computer controlled plotter works in a rectangular coordinate system a certain amount of error is unavoidable whilst plotting circular symmetric filters for defocusing. The double-phase hologram filters, due to coarse amplitude quantization, resulted in loss of resolution in the deblurred output. The DPH filter encoding only a square-root of the required Wiener filter amplitude transmittance, backed up by the photographically generated filter gave better resolved outputs.

One of the disadvantages of binary hologram filters is the high production costs involved, for filters meant for large objects take a very long plotting time. The high space-bandwidth product "natural hologram" resulting from optical heterodyning of the low space-bandwidth product was found suitable for processing large objects. The quality of the deblurred outputs from the heterodyned filter is very satisfactory (Chapte 6). Thus heterodyning is an effective means of keeping the plotting costs low when processing large objects.

REFERENCES

1. G.W.Stroke, 'Optical Computing', IEEE Spectrum, Vol.9., Dec. 1972, pp24-41.

2. J.L.Harris, 'Diffraction and resolving power', J.Opt.Soc.Am. Vol.54, July 1964, pp931-936. D.Slepian and H.O.Pollak, 'Prolate spheroidal wave functions, Fourier analysis and uncertainty-I', Bell Syst.Tech.J., Vol.40, 1963, pp67-87.

3. A.A.Sawchuk, 'Space-variant image motion degradation and restoration', Proc.IEEE, Vol.60, July 1972, pp854-861.

4. G.M.Robbins and T.S.Huang, 'Inverse filtering for linear shift-variant imaging systems', Proc.IEEE, Vol.60, July 1972, pp862-872.

5. O.Bryngdahl, 'Geometrical transformation in Optics', J.Opt.Soc. Am., Vol.64, Aug.1974, pp1092-1099.

6. D.Casasent, 'Optical Mellin transforms using computer generated holograms', Opt.Commun., Vol.19, Nov.1976, pp217-222.

7. S.Slepian, 'Restoration of photographgs blurred by image motion', Bell Sys.Tech.J., Vol.46, Dec.1967, pp2353-2362.

8. C.W.Helstrom, 'Image restoration by the method of least squares', J.Opt.Soc.Am., Vol.57, Mar.1967, pp 297-303.

9. C.W.Barnes, 'Object restoration in a diffraction-limited imaging system', J.Opt.Soc.Am., Vol.56, May 1966, pp575-578.

10. J.L.Harris Sr., 'Image evaluation and restoration', J.Opt.Soc. Am., Vol.56, May 1966, pp569-574.

11. J.L.Horner, 'Optical restoration of image blurred by atmospheric turbulence using optimum filter theory', Appl.Opt., Vol.10, Jan, 1970, pp167-171.

12. G.W.Stroke and R.G.Zech, '*A posteriori* image-correcting deconvolution by holographic Fourier-transform division', Phys.Lett., Vol.25A, July 1967, pp89-90.

13. A.W.Lohmann and H.W.Werlich, 'Holographic production of spatial filters for code translation and image restoration', Phys.Lett., Vol.25A, 1967, pp570-571.

14. A.Vander Lugt, 'Coherent optical processing', Proc.IEEE, Vol.62, Oct.1974, pp 1300-1318.

15. T.S.Huang, D.A.Barker and S.P.Berger, 'Iterative image restoration' Appl.Opt., Vol.14, May 1975, pp.1165-8.

16. P.A.Jansson, R.H.Hunt and E.K.Plyler, 'Resolution enhancement of spectra', J.Opt.Soc.Am., Vol.60, May 1970, pp596-599.

17. J.W.Cooley and J.W.Tukey,'An algorithm for the machine calculation of complex Fourier series', Math.Comput., Vol.19, 1965, pp297-301.

18. G.L.Rogers,'Noncoherent optical processing', John Wiley & Sons, New York, 1977, pp18-25.

19. F.Naderi and A.A.Sawchuk,'Estimation of images degraded by film-grain noise', Appl.Opt., Vol.17, 15 April 1978, pp1228-1237.

20. N.Wiener, 'Extrapolation,interpolation and smoothing time series', Technology press and Wiley, New York 1949.

21. D.Gorlitz and F.Lanzl, 'Methods of zero-order noncoherent filtering', Opt.Commun., Vol.20, Jan.1977, pp68 - 72.

22. G.L.Rogers and J.C.Davies, 'Noncoherent deconvolution', Opt. Commun., Vol.21, May 1977, pp311-317.

23. A.W.Lohmann, 'Incoherent optical processing of complex data', Appl.Opt., Vol.16, Feb.1977, pp261-263.

24. W.T.Rhodes, 'Bipolar pointspread function synthesis by phase-switching', Appl.Opt.,Vol.16, Feb.1977, pp265-267.

25. W.Stoner, 'Incoherent optical processing via spatially offset pupil masks', Appl.Opt.,Vol.17, 1 Aug.1978, pp2454-2467.

26. E.Abbe, Archiv.Mikroshopische Anat., Vol.9, 1873, p413.

27. F.Zernicke, 'Das phasenkontrastverfahren bei der mikroskopischen beobachtung', Z.Tech.Phys., Vol.16, 1935, p454.

28. A.Maréchal and P.Croce, 'Un filtre de frequences spatiales pour l'amelioration du contraste des images optique', C.R.Acad.Sci., Vol.127, Sept.1953, pp607-609.

29. J.Tsujiuchi, 'Correction of optical images by compensation of aberrations and by spatial frequency filtering', 'Progress in Optics' Vol.II, E.Wolf,Ed., North Holland 1963, pp131-180.

30. T.M.Holladay and J.D.Gallatin, 'Phase control by polarization in coherent spatial filtering', J.Opt.Soc.Amer.,Vol.56, July 1966,pp869-872.

31. G.D.Mountain, 'Photo-resist spatial filters for image enhancement', paper presented at the Institute of Physics meeting, Imperial College, London, Jan.1979.

32. G.W.Stroke, G.Indebetouw and C.Puech, '*A posteriori* holographic sharp-focus image-restoration from ordinary blurred photographs of 3-d objects photographed in ordinary white light', Phys. Lett., Vol.26A, Sept.1968, pp433-4.

33. G.W.Stroke, M.Halioua, G.Indebetouw and F.Poisson, 'Spatial domain laser light scanning deconvolution of blurred photographs using the general holographic deblurring filter, Opt. Commun.,Vol.1, March 1970, pp355-6.

34. G.W.Stroke and M.Halioua,'A new holographic image deblurring method', Phys.Lett.,Vol.33A, Jan.1970, pp3-4.

35. J.Perina, 'Holographic method of deconvolution and analytic continuation', Czech.J.Phys.,Vol.21B, July 1971, pp731-48.

36. G.W.Stroke and M.Halioua,'Image deblurring by holographic deconvolution with partially coherent low-contrast objects and application to electron microscopy', Optik, Vol.35, May 1972, pp489-508.

37. A.Vander Lugt,'Signal detection by complex spatial filtering', IEEE Trans.Inform.Theory, Vol.IT-10, Apr.1964, pp139-145.

38. G.W.Stroke, 'Image deblurring and aperture synthesis using *a posteriori* processing by Fourier transform holography', Opt. Acta , Vol.16, Apr.1969, pp401-422.

39. J.Tsujiuchi, T.Honda and T.Fukaya, 'Restoration of blurred photographic images by holography', Opt.Commun.,Vol.1, Aug.1970, pp379-82.

40. G.A.Krusos, S.K.Hilal, W.B.Seaman and G.W.Myers, 'Reduction of penumbra in X-ray imaging by optical spatial filtering', Appl. Phys. Lett.,Vol.16, 15 Jan 1970, pp37-40.

41. G.W.Stroke and M.Halioua, 'A new method for rapid realization of high-resolution extended-range holographic image-deblurring filter', Phys.Lett.,Vol.39A, May 1972, pp269-70.

42. J.W.Goodman and H.B.Strubin, 'Increasing the dynamic range of coherent optical filters by means of modulating gratings', J.Opt. Soc.Am., Vol.63,Jan.1973, pp50-58.

43. T.Minemoto, Y.Suemoto and S.Fudita, 'Holographic deblurring filter made with a flying-spot scanner exposure device', Jap. J.Appl.Phys., Vol.13, June 1974, pp975-83.

44. S.I.Ragnarsson, 'A new holographic method of generating high-frequency, extended range spatial filter with application to restoration of defocussed images', Phys.Scripta, Vol.2, No 4 - 5 1970, pp145-53.

45. A.W.Lohmann and D.P.Paris, 'Computer generated spatial filters for coherent optical data processing', Appl.Opt., Vol.7, Apr. 1968, pp651-5.

46. A.A.Friesem and D.Peri,'Coherent Optical image deblurring using computer generated holograms', Opt.Commun.,Vol.19, Dec. 1976, pp382-386.

47. P.Chavel and S.Lowenthal, 'A method of incoherent optical-image processing using synthetic holograms', J.Opt.Soc.Am., Vol.66, Jan. 1976, pp 14 - 23.

48. J.Tsujiuchi, S.Ishigura and T.Honda,'Image processing by multiple aperture scanning', Opt.Acta, Vol.21,Aug. 1974, pp 653-73.

49. L.Fleuret, H.Maitre and E.Cheval,'Image deblurring by convolution with an impule response operation', Opt.Commun.,Vol.21, June 1977, pp 361-4.

50. D.Peri and A.A.Friesem, 'Image restoration using volume diffraction gratings', Opt.Lett., Vol.3, Oct.1978, pp 124-126. Also see
S.K.Case, 'Fourier processing in the object plane', Opt.Lett., Vol.4, Sep.1979, pp 286-288.

51. P.Chavel and S.Lowenthal, 'Noise and coherence in optical processing. I - The Callier effect and its influence on image contrast', J.Opt.Soc.Am., Vol.68, May 1978, pp 559-568.

52. P.Chavel and S.Lowenthal , 'Noise and coherence in optical processing. II-Noise fluctuations', J.Opt.,Soc.Am., Vol.68, June 1978, pp 721 - 32.

53. D.Casasent and C.Szezutkowski, Opt. Commun.,'Optical Mellin transforms using computer generated holograms', Vol.19, Nov.1976, pp 217-22.

54. R.S.Sirohi and V.Ram Mohan, 'Differentiation by spatial filtering', Opt.Acta, Vol.24, Nov.1977, pp 1105 - 13.

55. E.N.Leith and J.Upatnieks, 'Reconstructed wavefronts and communication theory', J.Opt. Soc.Am., Vol.52, Oct. 1962,pp 1123-30.

56. A.W.Lohmann and D.P.Paris, 'Binary Fraunhofer holograms generated by computer', Appl.Opt., Vol.6, Oct.1967, pp 1739-48.

57. G.W.Stroke, M.Halioua and V.Srinivasan, 'Holographic image restroation using Fourier spectrum analysis of blurred photographs in Computer-aided synthesis of Wiener filters', Phys.Lett.,Vol.51A, 21.Apr.1975, pp383-5.

58. M.Jacobs, 'The production and separation of pulse width modulated carrier wave picture', a Final Year Student Project Report, Physics Department, University of Aston in Birmingham, June 1973.

59. G.L.Rogers,'Artificial holograms and astigmatism', Proc.R.Soc. Edinburgh, Vol.63A, Dec. 1951, pp 313 - 325.

60. C.K.Hsueh and A.A.Sawchuk, 'Computer-generated double-phase holograms', Appl.Opt., Vol.17, Dec.1978, pp 3874-3883.

61. D.C.Chu and J.W.Goodman, 'Spectrum shaping with parity sequences', Appl.Opt., Vol.11, Aug.1972, pp1716-24.

62. C.L.Miles, 'The production of Fresnel and sine wave zone-plates', App.Opt., Vol.7, May 1968, pp 976 - 7.

63. W.H.Lee, 'Binary synthetic holograms', Appl.Opt., Vol.13, July 1974, pp 1677 - 1682.

64. C.B.Burckhardt, 'A simplification of Lee's method of generating holograms by computer', Appl.Opt., Vol.9, Aug.1970, p1949.

65. J.C.Davies, 'Studies in deblurring with special reference to computer simulation', Ph.D.Thesis, Dept.of Phys. Aston Univ. Birmingham, U.K. 1976.

66. E.T.Whittaker, 'On the functions which are represented by the expansion of the interpolation theory', Proc.Roy.Soc.Edinburgh, Vol.35A, 1915, p181. C.E.Schannon 'Communication in the presence of noise', Proc.IRE, Jan.1949, pp10-21.

67. G.B.Anderson and T.S.Huang, 'Errors in frequency processing of images', 1969 Spring Joint Computer Conference, AFIPS Conf.Proc., Vol.34, pp173-185.

68. J.W.Goodman and A.M.Silvestri, 'Some effects of Fourier domain phase quantization', IBM J.Res.Develop., Vol. 14, Sept.1970, pp478-484.